cubation first with alkaline phosphatase–conjugated antibodies to digoxigenin and then with 5-bromo-4-chloro-3 indolyl-phosphate and 4-nitroblue tetrazolium chloride (Roche Diagnostics). The specimens were finally counterstained with hematoxylin.

RT-PCR. Transcripts encoding EP1, EP2, EP3, EP4, VEGF, CD31, and glyceraldehyde-3-phosphate dehydrogenase (GAPDH) were quantified by RT-PCR analysis. Tissue was removed and rapidly frozen in liquid nitrogen. The frozen tissue was pulverized in a stainless steel cylinder cooled with liquid nitrogen. Total RNA was extracted from the tissue with ISOGEN (Wako), and cDNA was synthesized from 1 μg of total RNA with the use of an oligo-p(dT)15 primer and AMV reverse transcriptase (Boehringer). 50 ng of cDNA were amplified with 1 U of Taq DNA polymerase in a 25 μl reaction mixture containing 10 mM Tris-HCl (pH 8.3), 50 mM KCl, 1.5 mM $MgCl_2$, 0.2 mM of each deoxynucleoside triphosphate, and 0.6 μM each of forward and reverse primers. The amplification protocol comprised 25 cycles (EP3, VEGF, CD31), 30 cycles (EP1), 40 cycles (EP2, EP4), or 20 cycles (GAPDH) of 45 s at 94°C, 60 s at 55°C, and 60 s at 72°C. The reaction mixtures were subsequently applied to a 2% agarose gel and the amplified products were stained with ethidium bromide. Primers used were as follows: 5′-AAT ACA TCT GTG GTG CTG CCA ACA-3′ (sense) and 5′-CCA CCA TTT CCA CAT CGT GTG CGT-3′ (antisense) for EP1, 5′-AGG ACT TCG CAG CCC CTT ACA CTT CTC CAA TG-3′ (sense) and 5′-CAG CCC CTT ACA CTT CTC CAA ATG-3′, 5′-GGA GAG ACT CAG TGA AGA AAT ATC-3′ (antisense) for EP2, 5′-GGAGAGACTCAGTGCA-GAAATATC-3′ (sense) and 5′-GAACTGTTAGTGACAC-CTGGAATG-3′ (antisense) for EP3, 5′-TTC CGC TCG TGG TGC GAG TGT TTC-3′ (sense) and 5′-GAG GTG GTG TCT GCT TGG GTC AG-3′ for EP4, 5′-AACCAT-GAACTTTCTGCTCTC-3′ (sense) and 5′-GTGATTTTC-TGGCTTTGTTC-3′ (antisense) for VEGF, 5′-CGGGATC-CAGGAAAGCCAAGGCCAAA-3′ (sense) and 5′-CGGAAT-TCTTGACTGTCTTAAGTTCC-3′ (antisense) for CD31, and 5′-CCCTTCATTGACCTCAACTACAATGGT-3′ (sense) and 5′-GAGGGGCCATCCACAGTCTTCTG-3′ (antisense) for GAPDH.

Real Time RT-PCR. Isolation of RNA and reverse transcription was performed as described above. Before transcription, all RNA samples were treated with 1 μg of DNase I (Life Technologies) per 1 μg RNA. In addition, 2.5 μg RNA from each sample was not reverse transcribed to ensure the effectiveness of the DNase treatment. Aliquots of 12.5 μg of the cDNA and gene-specific primers were added to 25 μl of qPCR Mastermix for Syber Green I (Eurogentec). Amplification reaction was performed and analyzed on ABI Prism 7700 Sequence Detector (Applied Biosystems). Primers for murine desmin were 5′-TCC CCG CTG AGC TCT CCC GTG TT-3′ (sense) and 5′-AGC TCG CGC ATC TCC TCC TCG TAG-3′ (antisense). Above mentioned primers for CD31 were also used. mRNA levels were normalized to β-actin mRNA and are presented as a ratio of desmin mRNA expression to CD31 mRNA.

Northern Blot Analysis. Total RNA (20 μg) extracted from tissue as described above was fractionated by electrophoresis on a 1% agarose gel containing 2.2 M formaldehyde. The separated RNA molecules were transferred and covalently bound by alkaline fixation and ultraviolet radiation–induced cross-linking to a Hybond-N+ membrane (Amersham Biosciences). For preparation of mouse VEGF and GAPDH cRNA probes, 427- and 470-bp fragments of the respective cDNAs were cloned from RAW246.7 cells and subcloned into the pGEM-T Easy vector (Promega). Plasmid DNA containing these fragments was linearized with NcoI or SalI, respectively, and then used as a template for synthesis of cRNA probes labeled with digoxigenin-UTP (Roche Diagnostics) by in vitro transcription with SP6 or T7 RNA polymerase. The presence of cRNA probes hybridized with mRNA on the membrane was detected with the use of alkaline phosphatase–conjugated antibodies to digoxigenin and the substrate CDP-Star (Roche Diagnostics). The membrane was exposed to x-ray film for visualization of chemiluminescence signals.

Gel Shift Assay. Primary cultured stromal fibroblasts of EP3 WT and EP3-knock out mice were stimulated with or without ONO-AE-248 (300 nM) in DMEM containing 10% FCS for 1 h. Double-stranded oligonucleotides containing consensus sequences were labeled with digoxigenin-11-ddUTP (Roche Diagnostics). The sense sequence of synthesized oligonucleotides used was 5′-CGC TTG ATG AGT CAG CCG GAA-3′. 20 μg of the nuclear extracts of fibroblasts (passage 3) were incubated with 0.155 pmol of DIG-labeled AP-1 oligonucleotide in binding buffer (10 mM HEPES, 50 mM KCl, 5 mM $MgCl_2$, 0.5 mM EDTA, 5 mM DTT, 0.7 mM PMSF, 1 mg/ml poly(dI-dC)poly(dI-dC), pH 7.9) for 15 min at 25°C. For competition assay, 100-fold excess of unlabeled oligonucleotide was added to the binding reaction to the addition of the DIG-labeled probe. Then these incubation mixtures added electrophoresed in 6% native polyacrylamide gels with Tris borate-EDTA buffer. Detection of chemiluminescence was performed by using Gel Shift kit (Roche Diagnostics).

Drugs. Aspirin was provided by Merck, NS-398 (22) was obtained from Cayman Chemical, SC-560 (23) was provided by Searle (Skokie, IL), and JTE-522 (24) was kindly supplied by Japan Tobacco (Tokyo, Japan). EP receptor selective agonists, ONO-DI-004, ONO-AEI-257, ONO-AE-248, and ONO-AEI-329, which were developed by us previously (18), were topically injected to the sponges. An orally active, low molecular weight inhibitor of VEGF receptor (KDR/VEGFR 2) tyrosine kinase (ZD6474) (25) was a gift from AstraZeneca (Cheshire, UK).

We newly developed an EP3 antagonist, ONO-AE3–240. The Ki values of this antagonist obtained by competition-binding isotherms to displace the radioligand binding to the respective prostanoid receptor are 590, 0.23, 58, and 1,500 nM for EP1, EP3, EP4, and FP, respectively, and more than 10 mM for EP2, DP, TP, and IP. Analysis of the agonistic and antagonistic actions showed that this compound acts as a selective antagonist at EP3 receptors. This inhibited the PGE_2 (10 nM)-induced increase in cytosolic Ca^{2+} concentration with median inhibitory concentrations of 1.5 nM for mouse EP3 receptor. This compound was dissolved in absolute ethanol at concentrations of 50 mM and 15 mM, and this stock solutions were diluted 100 times with physiological saline immediately before the topical injections. 3 d after the implantation of S-180 cells, the diluted solutions (0.1 ml/site) were subcutaneously injected around the tumors for 11 d twice a day. Physiological saline containing 1% ethanol was injected as vehicle control. An EP1 antagonist (ONO-8711; reference 17), and an EP4 antagonist (ONO-AE3–208; reference 19) were also topically injected around the tumors (twice a day, 50 nmole per tumor), in the same manner as ONO-AE3–240.

Statistical Analysis. Data are expressed as means ± SEM. Comparisons among multiple groups were performed by factorial analysis of variance (ANOVA) followed by Scheffe's test. Comparisons between two groups were performed with Student's *t* test. A P value of <0.05 was considered statistically significant.

Results

The effects of COX inhibitors on tumor growth and angiogenesis were first tested using sarcoma 180 cells, which are allogeneic for ddy mice (Fig. 1). In control ddy mice treated with vehicle, solid tumors were apparent 14 d after cell implantation. Daily oral administration of SC-560, the inhibitor selectively acting on COX-1, had no significant effect on tumor mass. In contrast, the COX-2–selective inhibitors JTE-522 and NS-398 significantly reduced tumor mass, as did aspirin, a nonselective COX inhibitor (Fig. 1, A and D). The extent of tumor-induced angiogenesis was assessed on the basis of hemoglobin contents (Fig. 1 C), which correlated well with the vascular density in the tumor under histological examination (Fig. 1 B). Consistent with the marked red color of the tumors, angiogenesis was substantial in vehicle-treated mice (Fig. 1, B and C). Similar to the findings in tumor mass, angiogenesis was greatly reduced by treatment with COX-2 inhibitors or aspirin, but not with SC-560 (Fig. 1, B and C). These results suggested that COX-2 was involved in tumor growth and angiogenesis also in this model.

To test whether PGs generated by COX-2 are involved in angiogenesis and, if so, to identify a PG species and a PG receptor involved, we next employed a sponge implantation model that we developed previously. This model utilizes a polyurethane sponge implanted subcutaneously in mice, which induces proliferative granulation tissue around the implant and extensive angiogenesis within this encapsulation in a COX-2–dependent manner, thus mimicking the stromal angiogenic response around tumors. In the present experiment, to identify the receptor mediating the above action, we topically injected recently developed EP agonists that are highly selective for each subtypes. Neither the EP1 agonist ONO-DI-004, nor the EP2 agonist ONO-AEI-257, nor the EP4 agonist ONO-AEI-329 enhanced significant angiogenesis (Fig. 2 A). In contrast, the EP3 agonist ONO-AE-248 markedly increased the extent of angiogenesis in a dose-dependent manner (Fig. 2 A). Administration of ONO-AE-248 significantly increased the rate of angiogenesis, with the maximal effect at day 14 (Fig. 2 C). These were also true in the mice treated with a COX-2 selective inhibitor, JTE-522 (Fig. 2 B). These results suggest a role of the PGE_2-EP3 receptor signaling in the sponge-induced angiogenesis.

To verify the role of endogenous PGE_2, we applied the sponge model to mice deficient in EP3 receptor ($EP3^{-/-}$). We also used mice deficient in IP receptor ($IP^{-/-}$), because endogenous PGI_2 levels were increased in sponge implantation models. Their respective WT counterparts, were used as controls. The extent of angiogenesis in $EP3^{-/-}$ mice was significantly reduced compared with that in WT mice (Fig. 2 D). In contrast, angiogenesis was significantly enhanced in $IP^{-/-}$ mice compared with that in WT animals (unpublished data). The impaired angiogenic response in $EP3^{-/-}$ mice was due to loss of receptors and not due to a difference in the production of PGs, as the amounts of PGE_2 and 6-keto-$PGF1_\alpha$, a stable metabolite of PGI_2, in the sponge implants

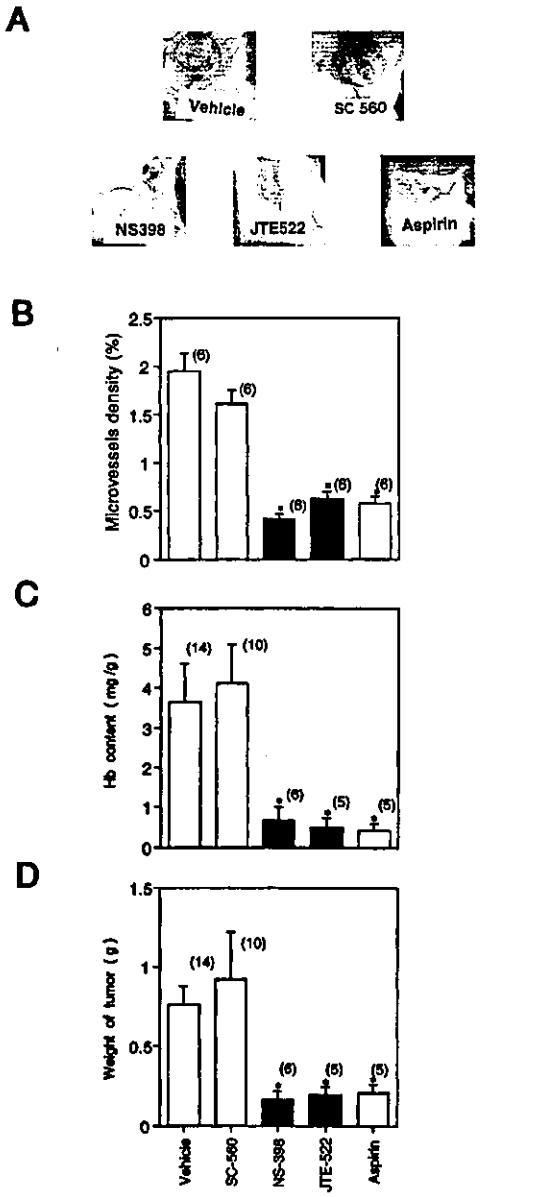

Figure 1. Effects of COX inhibitors on tumor growth and angiogenesis. (A) Typical appearance of tumors. A suspension of sarcoma 180 cells, which are allogeneic for ddy mice, was injected into subcutaneous tissue of ddy mice. COX inhibitors (SC-560, NS-398, and JTE-522, 3 mg/ml; aspirin, 10 mg/ml) were administered orally as a suspension (0.1 ml per 10 g of body mass) twice a day (every 12 h) beginning on the day of cell implantation and continuing throughout the 14-d experimental period. Tumors were then dissected and photographed. (B and C) The density of microvessels and hemoglobin content of tumor tissue were determined at the end of the 14-d experimental period. Data are means ± SEM for the indicated number of tumors. $^*P < 0.05$ versus vehicle-treated mice (ANOVA). (D) The mass of tumor tissue was determined at the end of the 14-d experimental period. All experiments were performed using male ddy mice. Data are means ± SEM for the indicated number of tumors. $^*P < 0.05$ versus vehicle-treated mice (ANOVA).

in $EP3^{-/-}$ mice (345 ± 67 and 299 ± 28 pg per sponge, $n = 6$, respectively) were not significantly different from those in WT mice (260 ± 46 and 255 ± 39 pg per sponge, $n = 6$, respectively). The expressions of VEGF in sponge granula-

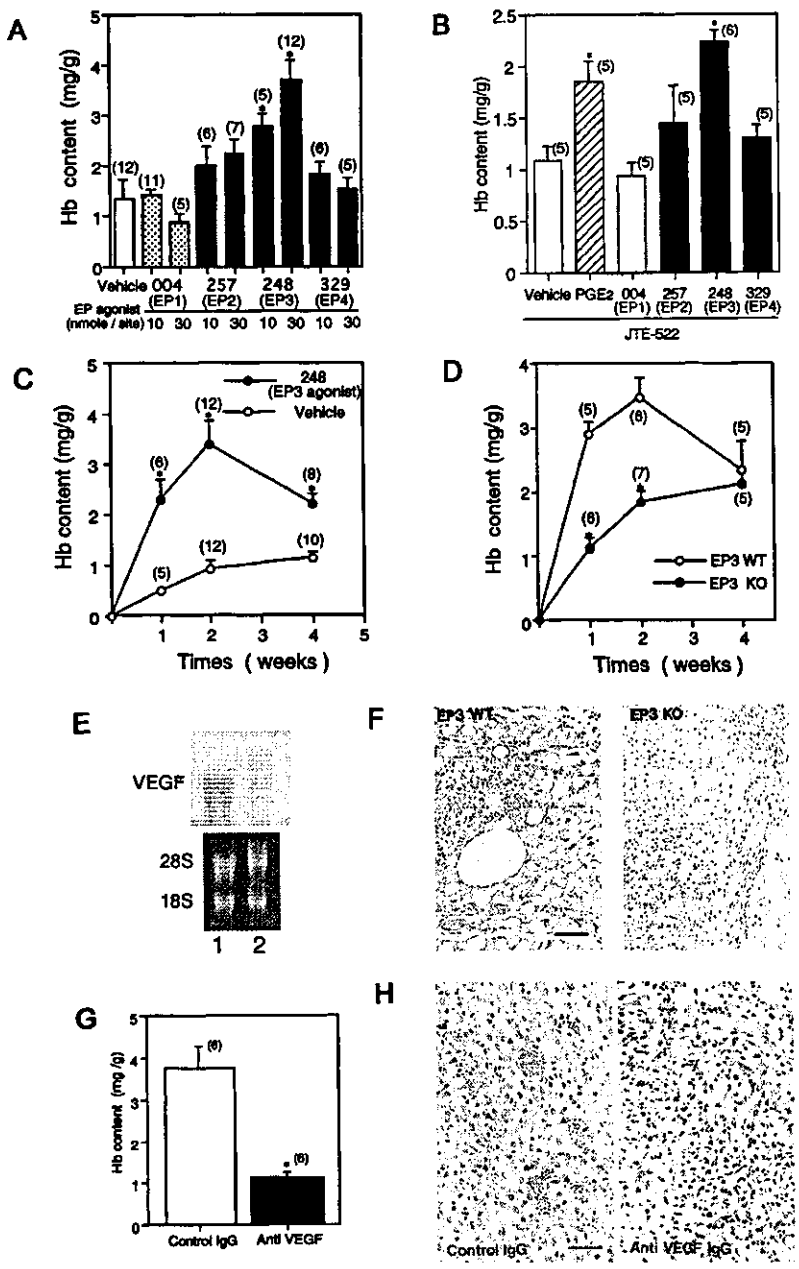

Figure 2. Angiogenesis in sponge-induced granulation tissues. (A) Hemoglobin content for male ddy mice treated with agonists selective for each EP subtype. ONO-DI-004 (EP1 agonist), ONO-AEI-257 (EP2 agonist), ONO-AE-248 (EP3 agonist), or ONO-AEI-329 (EP4 agonist) was topically injected into the implanted sponge over a period of 14 d (10 or 30 nmol per sponge per day) beginning on the day of implantation. Sponge-induced granulation tissue was dissected and its hemoglobin content was determined. Data are means ± SEM for the indicated number of sponges (shown in parentheses). *P < 0.05 versus vehicle-injected sponges (ANOVA). (B) Hemoglobin content for COX-2 inhibitor-treated ddy mice receiving topical injections of EP subtype agonist. Each agonist was topically injected into the sponge over a period of 14 d (30 nmol per sponge per day). Sponge-induced granulation tissue was dissected and its hemoglobin content was determined. Data are means ± SEM for the indicated number of sponges (shown in parentheses). *P < 0.05 versus vehicle-injected sponges (ANOVA). (C) Time courses of hemoglobin content during topical injections of an EP3 agonist, ONO-AE-248 (30 nmol per sponge per day). Data are means ± SEM for the indicated number of sponges implanted in subcutaneous tissues. *P < 0.05 versus corresponding value for vehicle-injected sponges (ANOVA). (D) Time courses of sponge angiogenesis in $EP3^{+/+}$ (WT) and $EP3^{-/-}$ (KO) mice. Data are means ± SEM for the indicated number of sponges. *P < 0.05 versus corresponding value for WT mice (ANOVA). (E) Northern blot analysis of VEGF mRNA. Sponge granulation tissue was isolated 14 d after the implantation in $EP3^{+/+}$ mice (lanes 1) and $EP3^{-/-}$ mice (lanes 2). Total RNA was prepared and subjected to Northern blot analysis of VEGF mRNA (top panel). The bottom panel also shows ethidium bromide staining of 28S and 18S mRNA. (F) Immunohistochemical localization of VEGF in sponge-induced granulation tissues. Sections of granulation tissue isolated from $EP3^{+/+}$ (EP3 WT) and $EP3^{-/-}$ (EP3 KO) mice 14 d after sponge implantation were stained with antibodies to VEGF. Scale bar, 50 μm. (G) Effects of topical injections with antibodies to VEGF on angiogenesis. Sponges were implanted to in C57BL/6 WT mice treated with the EP3 agonist (30 nmol per site per day) for 14 d. Sponges were also injected with either IgG specific for mouse VEGF (10 μg per sponge per day) or nonimmune control IgG. Data are means ± SEM for the indicated number of sponges. *P < 0.05 versus sponges injected with control IgG (Student's *t* test). (H) Effects of topical injections with antibodies to VEGF on angiogenesis. Hematoxylin-eosin staining of sections prepared from granulation tissues in C57BL/6 WT mice. The arrows indicate neovasculized vessels. Scale bar, 50 μm. The experiments were performed in male ddy mice (A–C), male $EP3^{-/-}$ and WT C57BL/6 mice (D–F), and male WT C57BL/6 mice (G and H).

tion tissues were markedly reduced in $EP3^{-/-}$ mice, compared with those in WT mice (Fig. 2, E and F). These results taken together demonstrate a significant role of endogenous PGE_2 in the sponge-induced angiogenesis, and suggest that EP3 receptor mediates this proangiogenic action of PGs. EP3 signaling is a major pathway for this angiogenesis, as topical injections of either EP3 agonist or PGE_2 did not enhance angiogenesis at all in $EP3^{-/-}$ mice (data not shown). Expressed VEGF certainly enhanced angiogenesis in this model, as VEGF antibody significantly reduced angiogenesis compared with control IgG (Fig. 2, G and H).

We then investigated whether the PGE_2-EP3 signaling also operates in tumor-induced angiogenesis by comparing tumor growth and angiogenesis in four kinds of EP receptor knockout mice, $IP^{-/-}$, and their WT counterparts injected with sarcoma 180 cells. Sarcoma 180 cells are allogeneic for the prostanoid receptor knockout mice, which was developed from C57BL/6 mice. Solid tumors that formed in $EP3^{-/-}$ mice were significantly smaller than those in WT mice (Fig. 3, B and D). Indeed, 14 d after the implantation of tumor cells, both tumor mass and angiogenesis, the latter assessed from microvessel density and hemoglobin

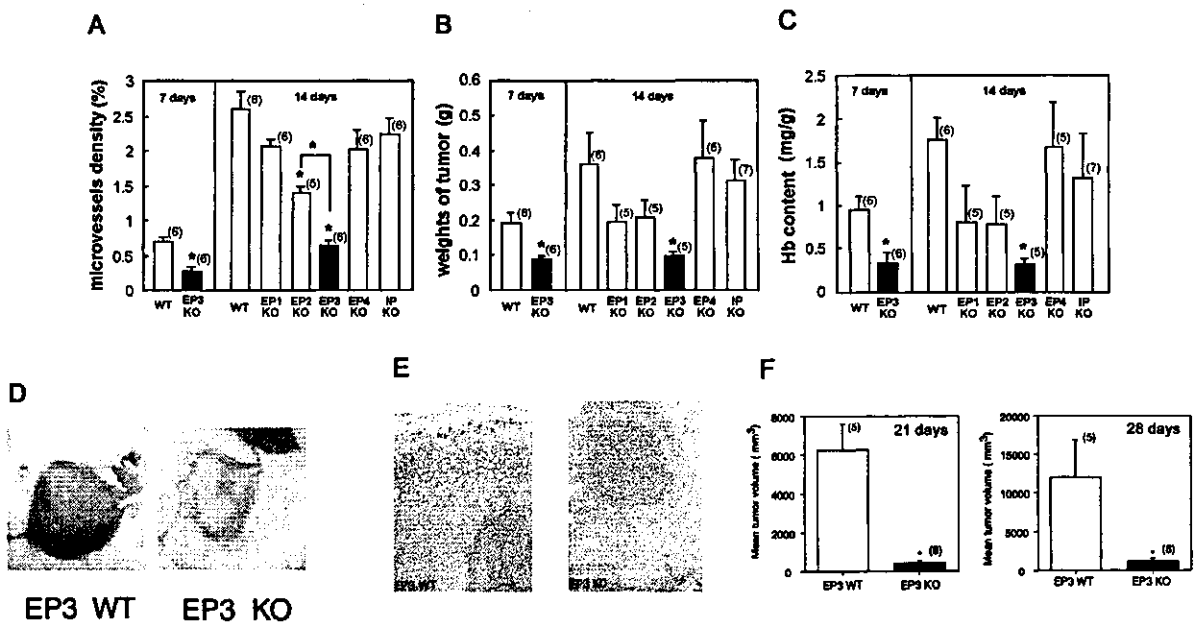

Figure 3. Tumor growth and angiogenesis in prostanoid receptor knockout mice. Sarcoma 180 cells, which are allogeneic for C57BL/6 mice, were injected to the subcutaneous tissue of the back except the experiment shown in panel F. (A and C) Tumor-associated angiogenesis was determined by the density of microvessels and hemoglobin content 7 and 14 d after injection of sarcoma 180 cells. (B) Tumor weight was also measured. Data are means ± SEM for the indicated number of tumors. *$P < 0.05$ versus corresponding value for WT mice (ANOVA). *$P < 0.05$, EP3 KO versus EP2 KO (Dunnett comparison). (D) Appearance of tumors. Tumors formed 14 d after injection of sarcoma 180 cells into (WT) and EP3$^{-/-}$ (KO) mice were dissected and photographed. (E) Hematoxylin-eosin staining of tumors from (WT) and EP3$^{-/-}$ (KO) mice. Scale bar, 100 μm. (F) Tumor mass assessed 21 and 28 d after injection of another tumor cell line, Lewis Lung carcinoma cells suspension (5×10^7 cells/ml, 100 μl/site) into the subcutaneous tissue of male mice. This cell line was syngeneic for C57BL/6 mice. The tumor volume was determined, as described before (reference 6). Data are means ± SEM for the indicated number of tumors. *$P < 0.05$ versus WT animals (Student's t test). All experiments were performed using male C57BL/6 mice with and without disruption of EP receptor subtypes or IP receptor.

content, were significantly reduced in EP3$^{-/-}$ mice compared with those in WT mice (Fig. 3 A–C). The extent of reduction in angiogenesis in EP3$^{-/-}$ (by 76%) was certainly larger than that observed in EP2$^{-/-}$ (by 46%), although angiogenesis in EP2$^{-/-}$ mice was also significantly reduced when assessed by microvessel density (Fig. 3 A). Even in the early stage of the experiment (7 d after implantation), the reduced angiogenesis and tumor growth were observed (Fig. 3, A–C). Fig. 3 D shows typical appearance of tumors formed in EP3$^{-/-}$ and WT mice. Histological examination of tumors formed in WT mice revealed an extensive vasculature in the capsule where tumors mingled with the surrounding normal tissue. In contrast, the tumors formed in EP3$^{-/-}$ mice exhibited both a low level of vascularization and distinct boundaries with the surrounding normal tissue (Fig. 3 E). We observed a difference of tumor growth between EP3$^{-/-}$ mice and WT mice using another neoplastic cell line, Lewis Lung carcinoma, which are syngeneic for C57BL/6 mice (Fig. 3 F). These results suggest that the EP3 receptor in the host has a major and critical role in tumor-induced angiogenesis and tumor growth. As shown below (see Fig. 5 A), the major EP receptor expressed in subcutaneous tissues in WT mice was EP3.

To corroborate the interaction between tumors (sarcoma 180) and the surrounding stroma, we examined COX-2 and VEGF expression in tumor and stromal tissue by immunohistochemical analysis in allogeneic models. Intense staining for COX-2 was apparent in sarcoma cells of tumors that formed in WT mice; less marked staining was also apparent in the stromal cells surrounding the tumors in these animals (Fig. 4 A, left). Substantial COX-2 immunoreactivity was also detected in the tumors together with stromal cells that formed in EP3$^{-/-}$ mice, although the extent of neovascularization in the capsular stroma was markedly reduced (Fig. 4 A, right). In WT mice, VEGF was abundant in surrounding stromal cells (Fig. 4 B, left), which major components were Mac-1 and CD3 double-negative fibroblast-like cells (Fig. 4, F and G), and was also present in smaller amounts in tumor cells (Fig. 4 B, left). The number of stromal cells, as well as of tumor cells, expressing VEGF was markedly reduced in EP3$^{-/-}$ mice (Fig. 4 B, right). In situ hybridization revealed that EP3 mRNA was localized in both sarcoma and stromal cells (Fig. 4 C), but not in endothelial cells (Fig. 4 D, arrowhead), in WT mice, but was apparent only in the sarcoma cells in EP3$^{-/-}$ mice (unpublished data).

RT-PCR analysis confirmed these findings on expression of VEGF and EP3 mRNA in tumor (sarcoma 180) and capsular stromal tissue (T+St) from WT mice and EP3$^{-/-}$ mice. The expressed levels of other PGE receptor subtypes, EP1, EP2, and EP4, in both T+St and control subcutaneous tissue (H) were not apparently different between EP3$^{-/-}$ mice and WT mice (Fig. 5 A). It further detected transcripts encoding CD31 in the tissue from WT mice but not

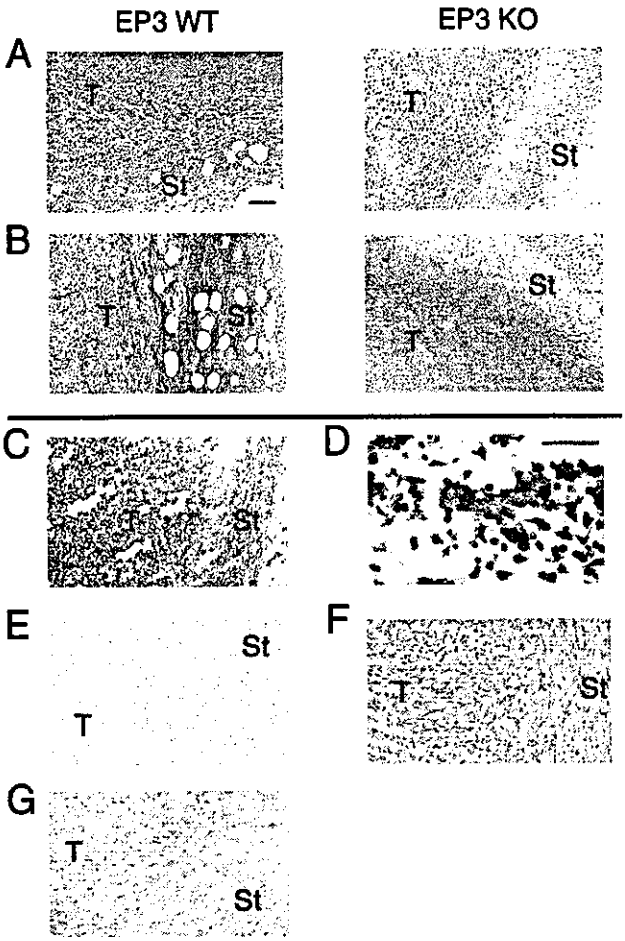

Figure 4. Expression of COX-2, VEGF, EP3 receptor in tumors and surrounding stroma tissues in WT mice and EP3 knockout mice 14 d after implantation of sarcoma 180 cells. (A) Immunohistochemical analysis of COX-2 expression in tumor (T) and stromal (St) tissue in WT $EP3^{+/+}$ (EP3 WT, left) and $EP3^{-/-}$ (EP3 KO, right) mice. COX-2 was apparent in both tumor cells and surrounding stromal cells, with no marked differences in the number of positive cells apparent between $EP3^{-/-}$ mice and their WT counterparts. Scale bar, 100 μm. (B) Immunohistochemical analysis of VEGF expression in tumor and stromal tissue in WT (left) and $EP3^{-/-}$ (right) mice. VEGF-positive cells were apparent in the marginal zone of the tumor and in the surrounding stromal cells. Staining was more intense in wild-type mice than in $EP3^{-/-}$ mice. (C–E) In situ hybridization analysis of EP3 mRNA in tumor and stromal tissue from WT mice. D, stromal tissue (high magnitude, scale bar 10 μm, arrowhead; neovascularization); E, results from control sense probe. (F) Immunohistochemical analysis of CD3e expression in tumor and stromal tissue in WT mice. (G) Immunohistochemical analysis of Mac-1 expression in tumor and stromal tissue in WT mice. All experiments were performed using male C57BL/6 mice with and without disruption of EP3 receptor. Sarcoma 180 cells, which are allogeneic for C57BL/6 mice, were injected to the subcutaneous tissues.

in that from $EP3^{-/-}$ mice (Fig. 5 A). The ratio of the expression of desmin mRNA to that of CD31 mRNA determined in the samples isolated from the normal subcutaneous tissue (H) was not different between $EP3^{-/-}$ mice and WT mice (Fig. 5 B). But, in the samples of sarcoma 180 tumors including surrounding stroma (T+ST), which were prepared in the same manner as PCR analysis experiment (Fig. 5 A), the ratio was reduced in both $EP3^{-/-}$ mice and WT mice, compared with that in the normal subcutaneous tissues isolated from each mouse (Fig. 5 B). Further, the reduction was more significant in $EP3^{-/-}$ mice in comparison with that in WT mice (Fig. 5 B).

Daily topical injections of VEGF antibody significantly reduced tumor growth and angiogenesis in WT mice, but not in $EP3^{-/-}$ mice, suggesting that VEGF is a predominant factor to induce tumor growth and angiogenesis in this model in response to EP3 signaling (Fig. 4 J). The lack of inhibition in tumor-associated angiogenesis in $EP3^{-/-}$ mice was also observed in the mice treated with the inhibitor of tyrosine kinase of VEGF receptor, which was effective in WT mice (Fig. 5 E).

Gel shift assays of several transcriptional factors (AP-1, AP-2, SP-1, HIF-1, NF-κB, and Oct-2A) in fibroblasts isolated from the stroma in $EP3^{-/-}$ mice and WT mice, revealed that of the factors tested, AP-1 activation was significantly reduced in $EP3^{-/-}$ mice, compared with WT mice, after stimulation with a selective agonist for EP3, ONO-AE-248 (Fig. 5 C). AP-1–dependent up-regulation of VEGF may be important in tumor-associated angiogenesis mediated by EP3 receptors.

Recently, we succeeded to develop a potent and selective EP3 antagonist, ONO-AE3–240. Daily topical injections of this EP3 antagonist around the tumor (sarcoma 180) significantly suppressed tumor-associated angiogenesis and tumor growth in WT mice, whereas those of an EP1 antagonist and an EP4 antagonist did not (Fig. 6 A). This chemopreventive effect of an EP3 antagonist was not seen in $EP3^{-/-}$ mice (Fig. 6 B).

Discussion

Treatment with NSAIDs limits tumor growth and metastatic potential in various model systems as well as clinically in cancer patients (26–29). Of the two COX isozymes, COX-2 appears to play the predominant role in tumor growth (2, 28, 29), although the underlying mechanism has remained unclear. The antiapoptotic potential of PGE_2 has been suggested to contribute to colorectal carcinogenesis (30). With the use of a synthetic antagonist specific for EP1 together with mice deficient in this receptor, Watanabe et al. (17) showed that EP1 contributes to the formation of precancerous lesions induced by the colon carcinogen azoxymethane. However, the effects of the antagonist and of receptor disruption were limited to partial inhibition, leaving open the possibility that additional COX-2–dependent mechanisms are important in carcinogenesis.

An important factor in the promotion of tumor growth is angiogenesis (31, 32). Substantial increases in tumor mass must be preceded by an increase in blood supply to provide the nutrients and oxygen required for tumor growth. It has been suggested that the mechanisms for promotion of angiogenesis are activated in the early stages of tumor development (33). We have now shown with our sarcoma 180 implantation model that COX-2–selective inhibitors inhibited tumor growth and associated angiogenesis. The COX-2 blockers inhibited tumor growth by ~80%, similar

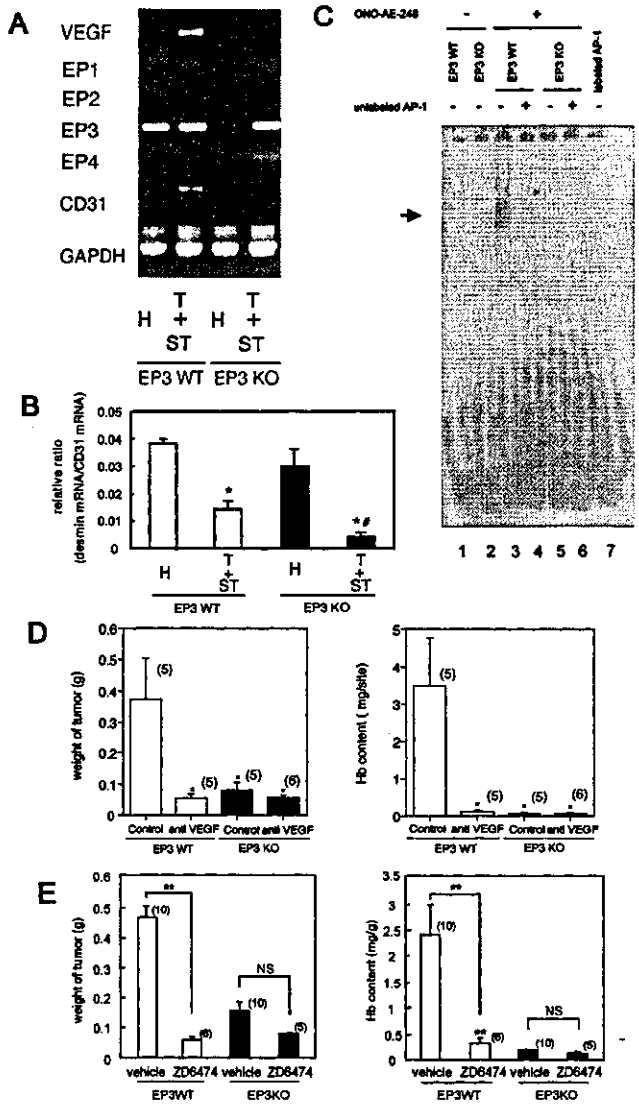

Figure 5. Expression of VEGF, EP receptor subtypes, and CD31 in tumors and surrounding stroma tissues in C57BL6 WT mice and EP3 knockout mice, and effects of a VEGF neutralizing antibody and a VEGF receptor kinase inhibitor on tumor growth and tumor-associated angiogenesis. Sarcoma 180 cells, which are allogeneic for C57BL/6 mice, were injected to the subcutaneous tissues. (A) RT-PCR analysis of EP1, EP2, EP3, EP4, VEGF, and CD31 mRNAs in tumor tissue dissected together with surrounding stroma (T + St), as well as in control subcutaneous tissue (H) dissected from sites distant from tumors, of WT and EP3$^{-/-}$ mice. 14 d after implantation, sample tissues were isolated. (B) A ratio of desmin mRNA/CD31 mRNA. Real time RT-PCR analysis was performed as described in the methods, and a ratio of the expression of desmin mRNA to that of CD31 mRNA was determined. Data are means ± SEM for 4 samples prepared as above. *P < 0.05 compared with H, and #P < 0.05 compared with T+ST in EP3WT (ANOVA). (C) Gel shift assay. Primary cultured fibroblasts from WT and EP3$^{-/-}$ mice were stimulated with ONO-AE-248, a EP3 agonist. Activation of AP-1 was determined by EMSA. Lanes 1, 2, and 7, or 3 to 6, without or with ONO-AE-248; lanes 4 and 6, presence of unlabeled oligonucleotide with nuclear extract, by which specificity was evaluated by oligonucleotide competition and EMSA; lane 7, control oligonucleotide without nuclear extract. (D and E) Effects of an anti-VEGF antibody and a VEGF receptor kinase inhibitor on tumor growth and angiogenesis in WT and EP3$^{-/-}$ mice. Tumor-associated angiogenesis was determined 14 d after injection of sarcoma 180 cells. Either IgG specific for mouse VEGF (10 μg per tumor per day, once a day) or nonimmune control IgG was topically injected around the tumors (D). Either VEGF receptor kinase inhibitor, ZD6474 (100 mg/kg, once a day) or vehicle control solution was orally administered (E). Data are means ± SEM for the indicated number of tumors. *P < 0.05 compared with WT mice receiving control IgG or vehicle solution (ANOVA).

to the extent of the effect of such inhibitors on the growth of COX-2–overexpressing tumor cells transplanted into nude mice (6). These latter researchers also showed that the promotion of tube formation by human umbilical vein endothelial cells induced by cocultured Caco-2 cells that overexpress COX-2 is mediated through the production and release of proangiogenic factors by the tumor cells themselves. If such a mechanism also operates in vivo, tumor-associated angiogenesis would depend only on tumor cells. However, we have now shown that not only angiogenesis but also tumor growth were significantly reduced in EP3$^{-/-}$ mice compared with those in WT mice, although the transplanted tumor cells expressed EP3 receptors. These results strongly suggested that the host stromal PGE_2-EP3 signaling was important in tumor-associated angiogenesis and tumor growth.

To mimic stromal angiogenic responses, we developed the sponge implantation model. Two advantages of this model for studies of angiogenesis are that angiogenesis can be readily quantified by measurement of the hemoglobin content of the sponge-induced granulation tissue together with histological examination, and that the effects of exogenous substances can be investigated by their direct injection into the sponge (7–9). The EP3 agonist ONO-AE-248 specifically enhanced angiogenesis in this model in a dose-dependent manner, and further the angiogenic response was certainly reduced in EP3$^{-/-}$ with the reduction of VEGF expression, suggesting that endogenous PGE_2 facilitates angiogenesis through the EP3 signaling and the induction of VEGF in this model. Previous studies with various cell lines have indicated that PGE_2 induces VEGF expression through a cAMP-dependent mechanism (34, 35). We previously reported that PGE_2 induces VEGF through the activation of adenylate cyclase/protein kinase A signaling pathway (36). One of the EP3 splicing variants (37, 38), which may couple to the elevation in intracellular cAMP levels, may enhance angiogenesis in this model.

It has been previously reported that E type PGs have a proangiogenic activity in corneal test (39) and in the chorioallantoic membrane (CAM) technique (40). Further, Form and Auerbach reported that PGE_2 strongly induced angiogenesis on CAM of 8-d-old chicken embryos, but PGA_2, $PGF_{2\alpha}$, and a derivative of TXA_2 did not. A recent report (41) described that the endothelial migration was mediated by COX-2 and TXA_2, but this experiment was performed using confluent monolayer endothelial cells stimulated with PMA. The authors also reported that corneal angiogenesis was suppressed with COX-2 inhibitor and TXA_2 antagonist, the former of which inhibited more strongly than the latter, suggesting the involvement of

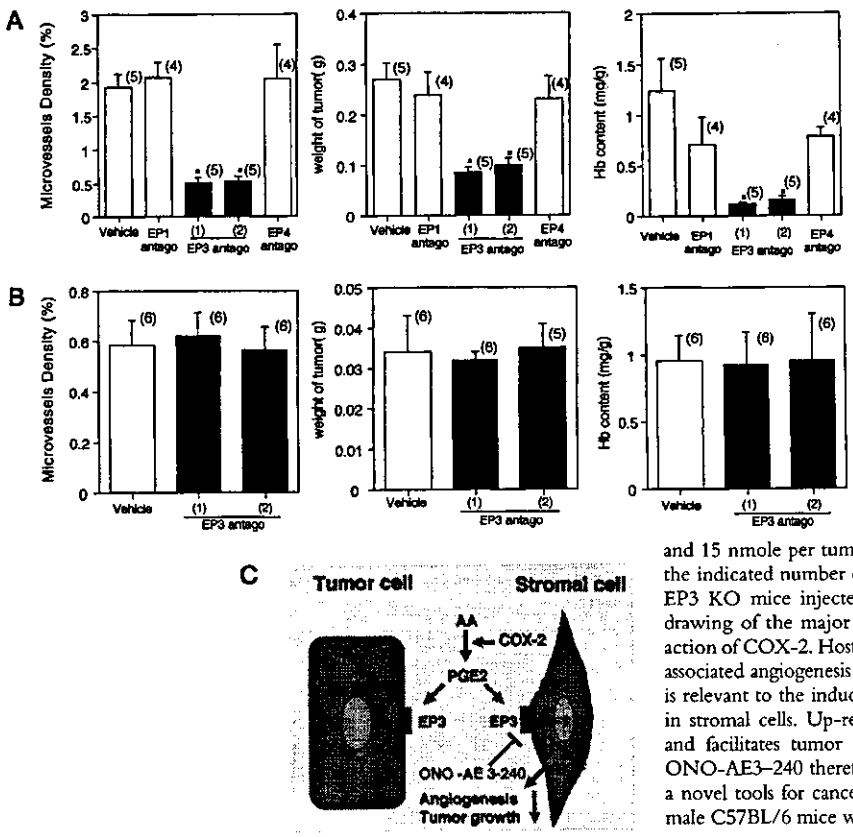

Figure 6. Effect of an EP3 antagonist on tumor growth and tumor-associated angiogenesis. Sarcoma 180 cells, which are allogeneic for C57BL/6 mice, were injected to the subcutaneous tissues. (A) Tumor-associated angiogenesis was determined in WT mice by the density of microvessels 14 d after the injection. Tumor weight was also determined 14 d after the injection. An EP1 antagonist (EP1 antago, ONO-8711), an EP3 antagonist (EP3 antago, ONO-AE3-240), or an EP4 antagonist (EP4 antago, ONO-AE3-208) was topically injected around the tumors (twice a day, 50 nmole per tumor). EP3 antago (1) and (2); twice a day, 50 and 15 nmole per tumor, respectively. Data are means ± SEM for the indicated number of tumors. $^*P < 0.05$ versus corresponding value for WT mice injected with vehicle solution (ANOVA). (B) Tumor growth and tumor-associated angiogenesis were determined in $EP3^{-/-}$ (KO) mice 14 d after injection of sarcoma 180 cells. An EP3 antagonist (ONO-AE3-240) was topically injected around the tumors. EP3 antago (1) and (2); 50 and 15 nmole per tumor per day, respectively. Data are means ± SEM for the indicated number of tumors. $^*P < 0.05$ versus corresponding value for EP3 KO mice injected with vehicle solution (ANOVA). (C) Schematic drawing of the major signaling pathway of PGE_2 generated through the action of COX-2. Host stromal PGE_2-EP3 signaling appears critical for tumor-associated angiogenesis and tumor growth. EP3 signaling on the stromal cells is relevant to the induction of a potent proangiogenic growth factor, VEGF in stromal cells. Up-regulated VEGF certainly has a proangiogenic action, and facilitates tumor growth. A highly selective EP3 antagonist such as ONO-AE3-240 therefore exhibits chemoprevetive action, and will become a novel tools for cancer prevention. All experiments were performed using male C57BL/6 mice with and without disruption of EP3 receptor.

other COX-2 products than TXA_2. However, these in vivo results were obtained under bFGF-stimulated conditions. In our separate experiment, angiogenesis in the sponge implantation model under no stimulation was not reduced with either a thromboxane synthase inhibitor, OKY046 or a TP receptor antagonist, S-1452 (unpublished data). The contribution of TP receptor signaling to tumor-associated angiogenesis should be estimated carefully. In the present experiments, we tested tumor-associated angiogenesis in knockout mice of EP subtypes or IP receptors (Fig. 3, A and C). As shown in the present study, not only tumor growth but also tumor-associated angiogenesis are highly dependent on EP3 receptor signaling. Judging from the time course of changes in size and angiogenesis of tumors in $EP3^{-/-}$ and WT mice (Fig. 3, A–C), the reduced tumor growth and angiogenesis in $EP3^{-/-}$ mice is not a simply minor delay. However, angiogenesis and growth of polyps in mice with a mutated APC gene were recently reported to be EP2-dependent (42, 43). Their report described that the major elements which express COX-2 are stromal cells around the tumors or intestinal polyps. We identified that the cells which produced VEGF to facilitate angiogenesis and tumor growth were CD3 and Mac-1 double-negative fibroblasts. It is widely known that the fibroblasts exhibit heterogeneity in term of various biological factors including prostaglandin generating systems and receptor systems (44–46). We have shown in the present study, not only tumor growth but also tumor-associated angiogenesis are highly EP3 dependent. They did not show the microvessel density in $EP3^{-/-}$ with APC mutation in their recent report (43), and the reduction percentage of angiogenesis in APC-mutated $EP2^{-/-}$ mice was ~30% at best. As shown in Fig. 5 A, the major EP receptor expressed in subcutaneous tissues in WT mice was EP3, which did not expressed in the intestine (43). These suggested that tumor-associated angiogenesis may be regulated in a site-specific fashion, and may be related to the heterogeneity of the stromal fibroblasts.

The mouse strains, ddy mouse and C57BL/6 mouse are allogeneic for S-180 sarcoma cell line used in the present study. However, we tested another cell line, Lewis lung carcinoma, for which C57BL/6 mouse is syngeneic (Fig. 3 F). The difference of tumor growth in $EP3^{-/-}$ mice and WT counterparts was observable in both tumor cell lines. These suggested that EP3 receptor signaling to facilitate the tumor growth was important not only in allogeneic tumors but also in syngeneic tumors.

The host microenvironment is thought to influence tumor progression (47, 48). Examination of human colorectal cancer tissue has revealed marked COX-2 expression not only in cancer cells but also in inflammatory cells and fibroblasts that surround the cancer cells (34). Ohshima et al. (2) also showed that COX-2 is abundant in the stromal cells that surround intestinal polyps in mice with a mutated APC gene. Recent results using COX-2 knockout mice also supported the significance of stromal COX-2 in tumor-induced angiogenesis and tumor growth (49). In the present study, we have focused on the down-stream signal-

ing pathway after COX-2 induction. We detected marked VEGF immunoreactivity in host stromal cells, including fibroblast-like cells, that surrounded the implanted sarcoma cells in $EP3^{+/+}$ mice but not in the corresponding cells of $EP3^{-/-}$ mice, suggesting that these stromal cells express VEGF in response to activation of EP3 receptors by endogenous PGE_2. We therefore propose that COX-2 expressing stromal cells around the tumors and/or tumor cells themselves synthesize and release PGE_2 into the tumor microenvironment, and that PGE_2 then acts on the stromal cells expressing EP3 receptors to induce the production of proangiogenic factors and consequent angiogenesis.

It is interesting to see whether or not EP3 receptor signaling enhances the stability of the newly formed vessels by modulating periendothelial cells which invest the vessels. Desmin was reported to be expressed in the pericytes on the tumor blood vessels, where the loose association of pericytes with endothelium (50). We performed real time PCR to determine a ratio of the expression of desmin mRNA to that of CD31 mRNA (Fig. 5 B). As the expression of CD31 is dependent on the proliferation of the endothelial cells on newly formed vessels, it is plausible that this ratio neatly correlates with the development of investment of pericytes on the blood vessels. The ratio determined in the samples isolated from the normal subcutaneous tissue (H) was not different between $EP3^{-/-}$ mice and WT mice. But, in the samples of S-180 tumors including surrounding stroma (T+ST), the ratio was reduced in both $EP3^{-/-}$ mice and WT mice, compared with that in the normal subcutaneous tissues isolated from each mouse. Further, the reduction was more significant in $EP3^{-/-}$ mice in comparison with that in WT mice. These results taken together suggest that the development of pericytes on the newly formed vessels in association to tumors is EP3 receptor signaling-dependent, and that the equipment of the pericytes in the vessels (arterioles and venules) in normal tissues is not.

Among the various factors, VEGF may be a candidate to enhance angiogenesis in sponge model judging from the results using VEGF neutralizing antibody (Fig. 2, G and H). Further, daily topical injections of VEGF antibody significantly reduced tumor growth and angiogenesis in WT mice, but not in $EP3^{-/-}$ mice (Fig. 5 D), suggesting that VEGF is a predominant factor to induce tumor growth and angiogenesis in host microenviroment. The results from VEGF receptor tyrosine kinase inhibitor concrete this finding (Fig. 5 E).

Gel shift assays of several transcriptional factors in stromal fibroblasts, revealed that AP-1 activation was significantly reduced in $EP3^{-/-}$ mice, compared with $EP3^{+/+}$ mice with an EP3 agonist (Fig. 5 I), suggesting that AP-1–dependent up-regulation of VEGF may be important in tumor-associated angiogenesis mediated by EP3 receptors. AP-1–dependent VEGF expression was also reported in several kinds of cells (51, 52).

To concrete the results so far obtained with $EP3^{-/-}$ mice, we topically injected an EP3 receptor antagonist, which we recently developed. Daily topical injections of an EP3 antagonist to the subcutaneous tissues around the tumor, where functionally active EP3 receptors are localized, significantly suppressed tumor-associated angiogenesis and tumor growth in WT mice, whereas those of an EP1 antagonist and an EP4 antagonist did not (Fig. 6 A). This chemopreventive effect of an EP3 antagonist was not seen in $EP3^{-/-}$ mice (Fig. 6 B). These results certainly confirm the results from $EP3^{-/-}$ mice.

In conclusion, as shown in Fig. 6 C, host stromal PGE_2-EP3 signaling appears critical for tumor-associated angiogenesis and tumor growth. EP3 signaling on the stromal cells was relevant to the induction of a potent proangiogenic growth factor, VEGF in stromal cells. Up-regulated VEGF certainly has a proangiogenic action, and facilitates tumor growth. A highly selective EP3 antagonist therefore exhibits chemoprevetive action on the stromal cells, and will become a novel therapeutic tool for cancer. The results presented here neatly provide an answer to the question how NSAIDs prevent tumor development.

We thank Michiko Ogino, Keiko Nakamigawa, Osamu Katsumata, and Masaki Soma for technical assistance.

This work was supported by research grants (no. 12470529 and no. 12670094), by "High-tech Research Center" grant, and by Academic Frontier Project grant from the Ministry of Education, Culture, Sports, Science and Technology. This study was also supported by an Integrative Research Program of the Graduate School of Medical Science, Kitasato University, and by a grant from Terumo life science foundation.

Submitted: 13 August 2002
Revised: 2 December 2002
Accepted: 4 December 2002

References

1. Smalley, W., and R.N. Dubois. 1997. Colorectal cancer and non steroidal anti-inflammatory drugs. *Adv. Pharmacol.* 39:1–20.
2. Ohshima, M., J.E. Dinchuk, S.L. Kargman, H. Oshima, B. Hancock, E. Kwong, J.M. Trzaskos, J.F. Evans, and M.M. Taketo. 1996. Suppression of intestinal polyposis in $Apc^{\Delta 716}$ knockout mice by inhibition of cyclooxygenase 2 (COX-2). *Cell.* 87:803–809.
3. Marx, J. 2001. Cancer research. Anti-inflammatories inhibit cancer growth–but how? *Science.* 291:581–582.
4. Prescott, S.M., and R.L. White. 1996. Self-promotion? Intimate connections between APC and prostaglandin H synthase-2. *Cell.* 87:783–786.
5. Shiff, S.J., and B. Rigas. 1997. Nonsteroidal anti-inflammatory drugs and colorectal cancer: evolving concepts of their chemopreventive actions. *Gastroenterology.* 113:1992–1998.
6. Tsujii, M., S. Kawano, S. Tsuji, H. Sawaoka, H. Hori, and R.N. DuBois. 1998. Cyclooxygenase regulates angiogenesis induced by colon cancer cells. *Cell.* 93:705–716.
7. Majima, M., M. Isono, Y. Ikeda, I. Hayashi, K. Hatanaka, Y. Harada, O. Katsumata, S. Yamashina, M. Katori, and S. Yamamoto. 1997. Significant roles of inducible cyclooxygenase (COX)-2 in angiogenesis in rat sponge implants. *Jpn. J. Pharmacol.* 75:105–114.
8. Muramatsu, M., J. Katada, I. Hayashi, and M. Majima. 2000. Chymase as a proangiogenic factor. A possible involvement of chymase-angiotensin-dependent pathway in the hamster sponge angiogenesis model. *J. Biol. Chem.* 275:5545–5552.

9. Majima, M., I. Hayashi, M. Muramatsu, J. Katada, S. Yamashina, and M. Katori. 2000. Cyclooxygenase-2 enhances basic fibroblast growth factor-induced angiogenesis through the induction of vascular endothelial growth factor in rat sponge implants. *Br. J. Pharmacol.* 130:641–649.
10. Narumiya, S., Y. Sugimoto, and F. Ushikubi. 1999. Prostanoid receptors: structures, properties, and function. *Physiol. Rev.* 79:1193–1226.
11. Murata, T., F. Ushikubi, T. Matsuoka, M. Hirata, A. Yamasaki, Y Sugimoto, A. Ichikawa, Y. Aze, T. Tanaka, N. Yoshida, A. Ueno, S. Oh-ishi, and S. Narumiya. 1997. Altered pain perception and inflammatory responses in mice lacking prostacyclin receptor. *Nature.* 388:678–682.
12. Sugimoto, Y., A. Yamasaki, E. Segi, K. Tsuboi, Y. Aze, T. Nishimura, H. Oida, N. Yoshida, T. Tanaka, M. Katsuyama, et al. 1997. Failure of parturition in mice lacking the prostaglandin F receptor. *Science.* 277:681–683.
13. Segi, E., Y. Sugimoto, A. Yamasaki, Y. Aze, H. Oida, T. Nishimura, T. Murata, F. Ushukubi, M. Fukumoto, T. Tanaka, et al. 1998. Patent ductus arteriosus and neonatal death in prostaglandin receptor EP4-deficient mice. *Biochem. Biophys. Res. Commun.* 246:7–12.
14. Ushikubi, F., E. Segi, Y. Sugimoto, T. Murata, T. Matsuoka, T. Kobayashi, H. Hizaki, K. Tuboi, M. Katsuyama, A. Ichikawa, et al. 1998. Impaired febrile response in mice lacking the prostaglandin E receptor subtype EP3. *Nature.* 395: 281–284.
15. Hizaki, H., E. Segi, Y. Sugimoto, M. Hirose, T. Saji, F. Ushikubi, T. Matsuoka, Y. Noda, T. Tanaka, N. Yoshida, et al. 1999. Abortive expansion of the cumulus and impaired fertility in mice lacking the prostaglandin E receptor subtype EP_2. *Proc. Natl. Acad. Sci. USA.* 96:10501–10506.
16. Matsuoka, T., M. Hirata, H. Tanaka, Y. Takahashi, T. Murata, K. Kabashima, Y. Sugimoto, T. Kobayashi, F. Ushikubi, Y. Aze, et al. 2000. Prostaglandin D_2 as a mediator of allergic asthma. *Science.* 287:2013–2017.
17. Watanabe, K., T. Kawamori, S. Nakatsugi, T. Ohta, S. Ohichida, H. Yamamoto, T. Matuyama, K. Kondo, F. Ushikubi, S. Narumiya, T. Sugimura, and K. Wakabayashi. 1999. Role of the prostaglandin E receptor subtype EP1 in colon carcinogenesis. *Cancer Res.* 59:5093–5096.
18. Suzawa, T., C. Miyaura, M. Inada, T. Maruyama, Y. Sugimoto, F. Ushikubi, A. Ichikawa, S. Narumiya, and T. Suda. 2000. The role of prostaglandin E receptor subtypes (EP1, EP2, EP3 and EP4) in bone resorption: an analysis using specific agonists for respective EPs. *Endocrinology.* 141:1554–1559.
19. Kabashima, K., T. Saji, T. Murata, M. Nagamachi, T. Matsuoka, E. Segi, K. Tsuboi, Y. Sugimoto, T. Kobayashi, Y. Miyachi, et al. 2002. The prostaglandin receptor EP4 suppresses colitis, mucosal damage and CD4 cell activation in the gut. *J. Clin. Invest.* 109:883–893.
20. Fujita, M., I. Hayashi, S. Yamashina, M. Itoman, and M. Majima. 2002. Blockade of angiotensin AT1a receptor signaling reduces tumor growth, angiogenesis, and metastasis. *Biochem. Biophys. Res. Commun.* 294:441–447.
21. Boku, K., T. Ohno, T. Saeki, H. Hayashi, I. Hayashi, M. Katori, T. Murata, S. Narumiya, K. Saigenji, and M. Majima. 2001. Adaptive cytoprotection mediated by prostaglandin I(2) is attributable to sensitization of CRGP-containing sensory nerves. *Gastroenterology.* 120:134–143.
22. Futaki, N., K. Yoshikawa, Y. Hamasaka, I. Arai, S. Higuchi, H. Iizuka, and S. Otomo. 1993. NS-398, a novel non-steroidal anti-inflammatory drug with potent analgesic and antipyretic effects, which causes minimal stomach lesions. *Gen. Pharmacol.* 24:105–110.
23. Smith, C.J., Y. Zhang, C.M. Koboldt, J. Muhammad, B.S. Zweifel, A. Shaffer, J.J. Talley, J.L. Masferrer, K. Seibert, and P.C. Isakson. 1998. Pharmacological analysis of cyclooxygenase-1 in inflammation. *Proc. Natl. Acad. Sci. USA.* 95:13313–13318.
24. Wakitani, K., T. Nanayama, M. Masaki, and M. Matsushita. 1998. Profile of JTE-522 as a human cyclooxygenase-2 inhibitor. *Jpn. J. Pharmacol.* 78:365–371.
25. Wedge, S.R., D.J. Ogilvie, M. Dukes, J. Kendrew, R. Chester, J.A. Jackson, S.J. Boffey, P.J. Valentine, J.O. Curwen, H.L. Musgrove, et al. 2002. ZD6474 inhibits vascular endothelial growth factor signaling, angiogenesis, and tumor growth following oral administration. *Cancer Res.* 62:4645–4655.
26. Tsujii, M., S. Kawano, and R.N. DuBois. 1997. Cyclooxygenase-2 expression in human colon cancer cells increases metastatic potential. *Proc. Natl. Acad. Sci. USA.* 94:3336–3340.
27. Masferrer, J.L., A. Koki, and K. Seibert. 1999. COX-2 inhibitors. A new class of antiangiogenic agents. *Ann. NY Acad. Sci.* 889:84–86.
28. Sawaoka, H., S. Tsuji, M. Tsujii, E.S. Gunawan, Y. Sasaki, S. Kawano, and M. Hori. 1999. Cyclooxygenase inhibitors suppress angiogenesis and reduce tumor growth in vivo. *Lab. Invest.* 79:1469–1477.
29. Williams, C.S., M. Mann, and R.N. DuBois. 1999. The role of cyclooxygenases in inflammation, cancer, and development. *Oncogene.* 18:7908–7916.
30. Tsujii, M., and R.N. DuBois. 1995. Alterations in cellular adhesion and apoptosis in epithelial cells overexpressing prostaglandin endoperoxide synthase-2. *Cell.* 83:493–501.
31. Folkman, J. 1971. Tumor angiogenesis: therapeutic implications. *N. Engl. J. Med.* 285:1182–1186.
32. Folkman, J. 1996. What is the evidence that tumors are angiogenesis dependent? *J. Natl. Cancer Inst.* 82:4–6.
33. Hanahan, D., and J. Folkman. 1996. Patterns and emerging mechanisms of angiogenic switch during tumorigenesis. *Cell.* 86:353–364.
34. Harada, S., J.A. Nagy, K.A. Sullivan, K.A. Thomas, N. Endo, G.A. Rodan, and S.B. Rodan. 1994. Induction of vascular endothelial growth factor expression by prostaglandin E_2 and E_1 in osteoblasts. *J. Clin. Invest.* 93:2490–2496.
35. Hoper, M.M., N.F. Voelkel, T.O. Bates, J.D. Allard, M. Horan, D. Shepherd, and R.M. Tuder. 1997. Prostaglandins induce vascular endothelial growth factor in a human monocytic cell line and rat lungs via cAMP. *Am. J. Respir. Cell Mol. Biol.* 17:748–756.
36. Amano, H., K. Ando, S. Minamida, I. Hayashi, M. Ogino, S. Yamashina, H. Yoshimura, and M. Majima. 2001. Adenylate cyclase/protein kinase A signaling pathway enhances angiogenesis through induction of vascular endothelial growth factor in vivo. *Jpn. J. Pharmacol.* 87:181–188.
37. Namba, T., Y. Sugimoto, M. Negishi, A. Irie, F. Ushikubi, A. Kakizuka, S. Ito, A. Ichikawa, and S. Narumiya. 1993. Alternative splicing of C-terminal tail of prostaglandin E receptor subtype EP3 determines G-protein specificity. *Nature.* 365:166–170.
38. Sugimoto, Y., M. Negishi, Y. Hayashi, T. Namba, A. Honda, A. Watabe, M. Hirata, S. Narumiya, and A. Ichikawa. 1993. Two isoforms of the EP3 receptor with dif-

ferent carboxy-terminal domains. Identical ligand binding properties and different coupling properties with Gi proteins. *J. Biol. Chem.* 268:2712–2718.
39. Ziche, M., J. Jones, and P.M. Gullino. 1982. Role of prostaglandin E1 and copper in angiogenesis. *J. Natl. Cancer Inst.* 69:475–482.
40. Spisni, E., F. Manica, and Y. Tomasi. 1992. Involvement of prostanoids in the regulation of angiogenesis by polypeptide growth factors. *Prostaglandins Leukot. Essent. Fatty Acids.* 47: 111–115.
41. Daniel, T.O., H. Liu, J.D. Morrow, B.C. Crews, and L.J. Marnett. 1999. Thromboxane A2 is a mediator of cyclooxygenase-2-dependent endothelial migration and angiogenesis. *Cancer Res.* 59:4574–4577.
42. Seno, H., M. Oshima, T.O. Ishikawa, H. Oshima, K. Takaku, T. Chiba, S. Narumiya, and M.M. Taketo. 2002. Cyclooxygenase 2- and prostaglandin E(2) receptor EP(2)-dependent angiogenesis in Apc(Delta716) mouse intestinal polyps. *Cancer Res.* 62:506–511.
43. Sonoshita, M., K. Takaku, N. Sasaki, Y. Sugimoto, F. Ushikubi, S. Narumiya, M. Oshima, and M.M. Taketo. 2001. Acceleration of intestinal polyposis through prostaglandin receptor EP2 in Apc(Delta 716) knockout mice. *Nat. Med.* 7:1048–1051.
44. Smith, T.J., G.D. Sempowski, H.S. Wang, P.J. Del Vecchio, S.D. Lippe, and R.P. Phipps. 1995. Evidence for cellular heterogeneity in primary cultures of human orbital fibroblasts. *J. Clin. Endocrinol. Metab.* 80:2620–2625.
45. Goldring S.R., M.L. Stephenson, E. Downie, S.M. Krane, and J.H. Korn. 1990. Heterogeneity in hormone responses and patterns of collagen synthesis in cloned dermal fibroblasts. *J. Clin. Invest.* 85:798–803.
46. Ko, S.D., R.C. Page, and A.S. Narayanan. 1977. Fibroblast heterogeneity and prostaglandin regulation of subpopulations. *Proc. Natl. Acad. Sci. USA.* 74:3429–3432.
47. Fukumura, D., F. Yuan, W.L. Monsky, Y. Chen, and R.K. Jain. 1997. Effect of host microenvironment on the microcirculation of human colon adenocarcinoma. *Am. J. Pathol.* 151:679–688.
48. Gohongi, T., D. Fukumura, Y. Boucher, C.O. Yun, G.A. Soff, C. Compton, T. Todoroki, and R.K. Jain. 1999. Tumor-host interactions in the gallbladder suppress distal angiogenesis and tumor growth: involvement of transforming growth factor beta. *Nat. Med.* 5:1203–1208.
49. Williams, C.S., M. Tsujii, J. Reese, S.K. Dey, and R.N. DuBois. 2000. Host cyclooxygenase-2 modulates carcinoma growth. *J. Clin. Invest.* 105:1589–1594.
50. Morikawa, S., P. Baluk, T. Kaidoh, A. Haskell, R.K. Jain, and D.M. McDonald. 2002. Abnormalities in pericytes on blood vessels and endothelial sprouts in tumors. *Am. J. Pathol.* 160:985–1000.
51. Hossain, M.A., C.M. Bouton, J. Pevsner, and J. Laterra. 2000. Induction of vascular endothelial growth factor in human astrocytes by lead. Involvement of a protein kinase C/activator protein-1 complex-dependent and hypoxia-inducible factor 1-independent signaling pathway. *J. Biol. Chem.* 275:27874–27882.
52. Park, J.S., L. Qiao, Z.Z. Su, D. Hinman, K. Willoughby, R. McKinstry, A. Yacoub, G.J. Duigou, C.S. Young, S. Grant, et al. 2001. Ionizing radiation modulates vascular endothelial growth factor (VEGF) expression through multiple mitogen activated protein kinase dependent pathways. *Oncogene.* 20: 3266–3280.

ORIGINAL ARTICLE

Taylor&Francis
healthsciences

Expanded Parietal Cell Pool in Transgenic Mice Unable to Synthesize Histamine

B. Hunyady, A. Zólyomi, J. Czimmer, G. Mózsik, T. Kozicz, E. Buzás, S. Tanaka, A. Ichikawa, A. Nagy, M. Palkovits & A. Falus

First Dept. of Medicine, Dept. of Radiology, Dept. of Human Development and Anatomy, Medical Faculty, University of Pécs, Pécs, Hungary; Dept. of Genetics, Cell and Immunobiology, Laboratory of Neuromorphology, First Dept. of Anatomy, Semmelweis University, Budapest, Hungary; Dept. of Physiological Chemistry, Graduate School of Pharmaceutical Sciences, Kyoto University, Kyoto, Japan; Dept. of Molecular and Medical Genetics, University of Toronto and Samuel Lunefeld Research Institute, Mount Sinai Hospital, Toronto, Canada

Hunyady B, Zólyomi A, Czimmer J, Mózsik G, Kozicz T, Buzás E, Tanaka S, Ichikawa A, Nagy A, Palkovits M, Falus A. Expanded parietal cell pool in transgenic mice unable to synthesize histamine. Scand J Gastroenterol 2003;38:133–140.

Background: The histidine decarboxylase enzyme (HDC) is responsible for the synthesis of histamine in mammals. Histidine decarboxylase-deficient ($HDC^{-/-}$) mice have recently been developed by targeted mutation of the HDC gene. **Methods:** The impact of prolonged histamine deficiency was studied on gastric morphology (by immunohistochemistry and morphometry), gastric acid secretion (by a wash-through method for basal gastric acid secretion and by pylorus ligation for stimulated gastric acid secretion) and gastrin levels (by radioimmunoassay) in homozygous $HDC^{-/-}$ mice kept on a low-histamine diet. **Results:** A double maximal gastric acid secretory response was found in knockouts after exogenous histamine administration. In contrast, the gastric acid secretion was significantly reduced after gastrinergic and cholinergic stimulation in the absence of histamine. The oxynthic gland area of $HDC^{-/-}$ mice was thickened with an increased parietal cell count compared to wild types. Substantially elevated serum and antral tissue gastrin levels of $HDC^{-/-}$ mice could be possible indications of both an expanded parietal cell mass and/or an increased histamine-induced maximal gastric acid secretory capacity of this genotype. **Conclusions:** These data suggest that not enough compensatory mechanisms develop in $HDC^{-/-}$ mice during a prolonged low-histamine diet to maintain/restore normal gastric acid secretion. An expanded parietal cell pool was also demonstrated in $HDC^{-/-}$ mice kept on a low-histamine diet, probably caused by a trophic effect of sustained hypergastrinaemia. The $HDC^{-/-}$ strain is a suitable model for studying the effects of achlorhydria and consequent hypergastrinaemia as an approach to human conditions such as atrophic gastritis or long-term antisecretory therapies.

Key words: Gastric acid secretion; gastrin; histamine; histidine decarboxylase enzyme; immunohistochemistry; transgenic mice

B. Hunyady, First Dept. of Medicine, Medical Faculty, University of Pécs, 13 Ifjúság u., HU-7643 Pécs, Hungary (fax. +36 72 536 148, e-mail. bhunyady@yahoo.com)

Physiological (basal and meal-stimulated) gastric acid secretion is governed primarily by stimulatory histaminergic, gastrinergic, cholinergic and inhibitory somatostatinergic mechanisms accomplished directly on acid-secreting parietal cells of the fundic stomach or indirectly on different regulatory elements of the gastric mucosa (1–3). Enterochromaffin-like cells and mucosal mast cells (major sources of histamine), antral G cells (producing gastrin), the enteric nervous system (cholinergic and non-cholinergic) and D cells (synthesizing somatostatin) are of particular interest from this aspect (4–6). Neither the interactions of these cells and modulators nor their individual contributions to gastric acid secretion are completely understood.

Transgenic mice, which lack the production of histamine, have recently been generated by targeted mutation of the gene of the histidine decarboxylase enzyme (HDC) (7), an enzyme that is known to be exclusively responsible for histamine production in mammals (8). Decreased numbers of mesenterial, subcutaneous and peritoneal mast cells, lack of compound 48/80 or dinitrophenol-induced permeability of ear vessels were observed in HDC targeted ($HDC^{-/-}$) mice compared to littermate wild types ($HDC^{+/+}$) (7). A comprehensive gastric acid secretory profile of these $HDC^{-/-}$ mice kept on a diet containing regular amounts of exogenous histamine has recently been published by our team (9).

In order to compare our previous studies in $HDC^{-/-}$ mice kept on a diet containing regular amounts of exogenous histamine (9), we tested the hypothesis that no recovery/escape route of gastric acid secretion develops in homozygous

Table I. Characteristics of the immunohistochemicals used in these studies

Primary antibody to	Host species	Dilution	Source
Histidine decarboxylase	Rabbit	1:2.000	Euro-Diagnostica, Malmo, Sweden
Histidine decarboxylase	Guinea pig	1:500	Euro-Diagnostica, Malmo, Sweden
Proton pump	Rabbit	1:1.000	Calbiochem-Novobiochem, La Jolla, Calif., USA
Chromogranin A	Rabbit	1:2.000	Dr. L. E. Eiden
Secondary antibody conjugates*	**Dilution**	**Catalog#**	
Anti-rabbit IgG – FITC	1:100	711-096-152	
Anti-rabbit IgG – Cy3	1:1000	711-166-152	
Anti-guinea pig IgG – FITC	1:100	706-096-148	
Anti-guinea pig IgG – Cy3	1:1.000	706-166-148	

*Affinity purified anti-IgG $F[ab']_2$ fragments (Jackson ImmonoResearch, West Grove, Pa., USA).

$HDC^{-/-}$ mice during a prolonged period of their lives when maintained on a low-histamine diet (after having grown up on a histamine-enriched diet). Although a study in mice kept on a low-histamine diet from birth could also provide valuable information, we decided to rear our animals on a histamine-enriched diet for three reasons. 1) Fertility, pregnancy and lactation of gestating mothers appear to be disturbed; mothers cannot therefore be restricted from histamine during pregnancy and lactation. 2) Withdrawal of histamine from birth might affect development of the animals in a complex way, and thus direct consequences on gastric physiology could be difficult to understand. 3) In our opinion, this model mimics the human condition where a normally developed stomach turns achlorhydric, as in the case of chronic inflammation or long-term antisecretory treatment. Histamine content of the stomach tissue has been reported as practically zero as early as after a 1-week period on a low-histamine diet in $HDC^{-/-}$ mice (7).

Materials and Methods

Animals

Adult (>9 months of age), male homozygous $HDC^{-/-}$ and $HDC^{+/+}$ mice (5–8 per group, weighing 25–35 g), genotyped as earlier (7) were used. The mice were housed under controlled light/dark conditions (lights on 0700–1900) at a room temperature of 23 ± 1°C. They were fed on a special histamine-enriched chow (8.9 mg histamine/g food) by their adult age. Thereafter they were kept on a low-histamine diet (<120 ng histamine/g food) for at least 6 weeks before study. The animal care regulations of the Semmelweis University, Budapest, Hungary were followed in all studies.

Gastric acid secretion

Gastric acid secretion was studied in anaesthetized mice (pentobarbital sodium, 5.5 mg/100 g from 5.5 mg/ml saline stock, intraperitoneal) fasted overnight in wire-bottomed cages prior to study with unlimited access to water.

Basal gastric acid secretion was investigated with a modified stomach wash-through method (10). The abdomen of anaesthetized mice was opened and the oesophagus ligated. From an incision on the duodenal bulb, a 2.4 mm outer diameter conical plastic tube was inserted into the stomach and the pylorus ligated with the tube inside (output drain). Using the tube, the stomach was quickly flushed with 1 ml of 0.15 M saline (pH 7.0); then, in 4 consecutive 15-min periods, the gastric acid produced was washed out and collected with 1 ml-s of the saline. Fifteen-minute samples were individually titrated to pH 7.0 with a measured amount of 0.01 M NaOH. The basal acid output was expressed as 10^{-7} mol H^+ per hour.

The effects of histamine, pentagastrin or bethanechol on gastric acid secretion were studied in pylorus ligated, anaesthetized mice (11, 12). The abdomen was opened and the pylorus was ligated. Immediately after surgery, one of the following secretory compounds was administered: histamine (0.6 mg/100 g from 0.6 mg/ml saline, subcutaneously), pentagastrin (50 µg/100 g from 50 µg/ml saline, subcutaneously), or bethanechol (15 µg/100 g from 30 µg/ml saline, intravenously through a jugular vein). Two hours later the animals were killed, the abdominal portion of the esophagi was clipped and the stomachs were removed. Over a tunneled tube, the stomachs were opened and washed through with 2 ml of 0.15 M saline (pH 7.0). The gastric acid output, expressed as 10^{-7} mol/h H^+, of each animal was determined by titrating the stomach washing fluids with 0.1 M NaOH to pH 7.0. Samples containing visible amounts of blood or food were not analysed; these animals were excluded.

To keep the need of $HDC^{-/-}$ mice reasonably low, the applicability and efficacy of several published acid-secretory regimens were piloted in fasted wild-type animals (13–18). Methods with a maximal acid-secretory response to each compound and with a less than 15% mortality in our hands were chosen. In wild-type animals, the above selected dose of histamine and pentagastrin produced a maximal acid secretory response. As for bethanechol, we were unable to increase the dose over 15 µg/100 g because of a high mortality. The response to this amount, however, was marked and consistent in wild types (data not shown).

Immunohistological methods

Immunohistochemical protocols described earlier (19–21) were followed in order to analyse parietal and endocrine cell

populations in the stomach of $HDC^{-/-}$ mice. Briefly, stomachs from animals perfused with 4% paraformaldehyde were either cryo-protected in 20% sucrose and frozen or embedded in paraffin. Cryostat sections (10 µm) or sections of paraffin embedded tissues (7 µm) were immunostained using primary antibodies to proton pump (HK; for parietal cells (22)), chromogranin A (CgA; for endocrine cells including ECL cells (23, 24)), and HDC enzyme, followed by Cy3- or FITC labelled secondary antibodies (Table I). Controls included stainings with non-immune sera and absorptions with the closest available rat histidine decarboxylase peptide (100 ng/ml), as described previously (19). Photomicrographs were taken using an Axiphot fluorescent microscope with filters for Cy3 and FITC (Zeiss, Germany).

Morphometric methods

Wet whole stomach weight, fundic mucosa thickness and parietal cell counts were analysed in morphometric studies. Thickness of the mucosa and parietal cell was studied in sections of paraffin-embedded tissues immunostained for HK. Cell counting was performed by an expert unaware of the genotype of the animal. Special efforts were made to count parietal cells in the greater curvature of the fundic mucosa, far from either the antrum or the forestomach, with gastric glands oriented perpendicularly to the surface. In such areas, whole mucosal thickness from the luminal surface down to the bottom of the lamina muscular mucosae was measured in three animals per group at least in three sections per animal and two different fields per section. Parietal cells were counted in the same fields, after taking photographs of equal

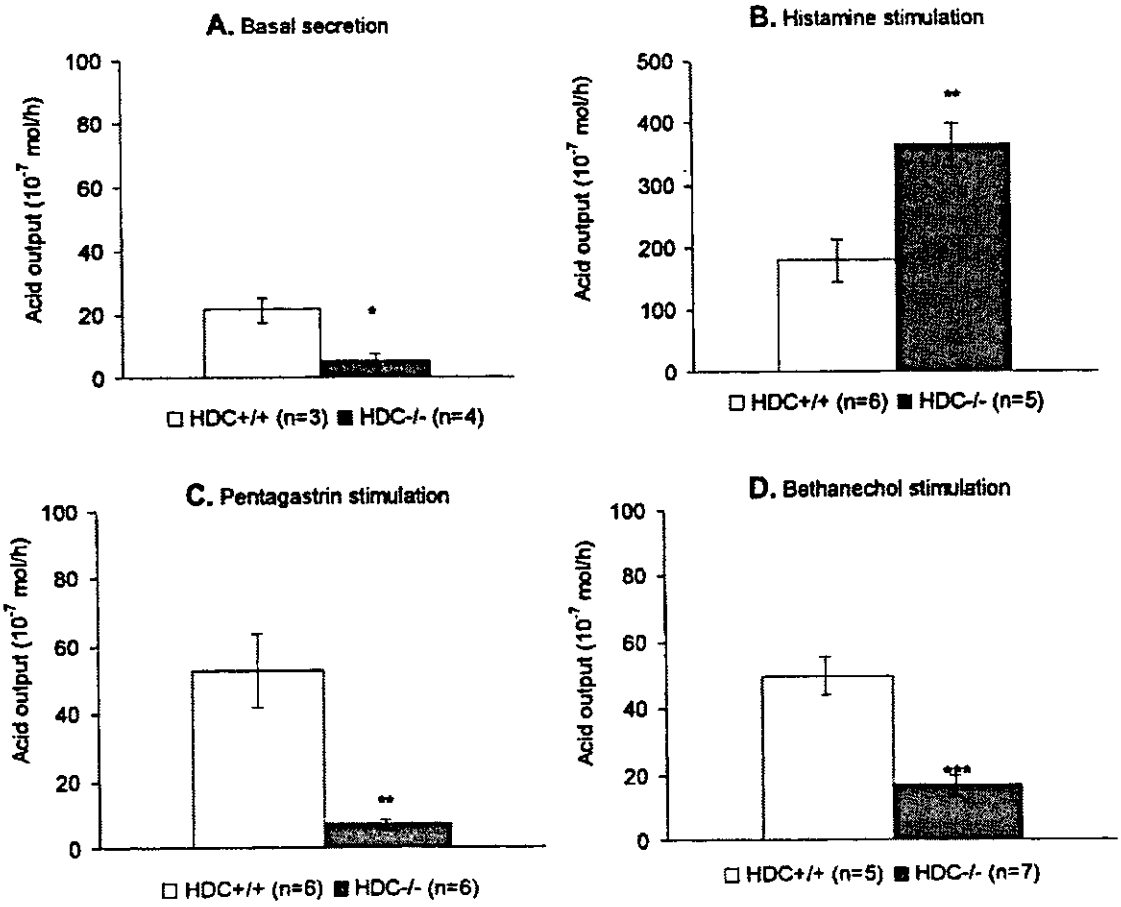

Fig. 1. Reduced basal gastric acid secretion, increased maximal gastric acid output after exogenous histamine stimulation and unresponsiveness to gastrinergic and cholinergic stimulants in histidine decarboxylase-deficient ($HDC^{-/-}$) mice. Panel A: Basal gastric acid output of $HDC^{-/-}$ mice ($n = 4$) is significantly reduced compared to $HDC^{+/+}$ animals ($n = 3$). Panel B: Increased maximal acid output of $HDC^{-/-}$ mice compared to $HDC^{+/+}$ after administration of exogenous histamine in a dose with maximal acid secretory response in normal mice (0.6 mg/100 g *sc*). Observe the difference in the scale of the y axis in Panel B as opposed to Panels A, C and D. Panels C and D: Virtually no acid output in $HDC^{-/-}$ mice after administration of pentagastrin (50 µg/100 g *sc*) or bethanechol (15 µg/100 g i.v.). This amount of pentagastrin and bethanechol caused marked gastric acid secretion in wild-type animals. $*P < 0.05$; $**P < 0.01$; $***P < 0.001$.

Table II. Morphometric data of $HDC^{-/-}$ and $HDC^{+/+}$ mice*

	$HDC^{-/-}$	$HDC^{+/+}$	$HDC^{-/-}$ $HDC^{+/+}$ ratio	Significance level
Body weight (g)	29.7 ± 0.8 (28.8–30.6; $n = 8$)	27.9 ± 0.9 (26.9–29.0; $n = 9$)	1.06	N.S.
Wet whole stomach weight (g)	0.31 ± 0.02 (0.29–0.33; $n = 8$)	0.26 ± 0.01 (0.24–0.28; $n = 9$)	1.19	$P < 0.05$
Mucosal thickness (mm)	0.54 ± 0.07 (0.50–0.58; $n = 23$)	0.43 ± 0.06 (0.38–0.48; $n = 25$)	1.26	$P < 0.01$
Parietal cell count (per field)	571 ± 9 (524–622; $n = 23$)	501 ± 8 (466–548; $n = 25$)	1.13	$P < 0.05$

*Results are expressed as mean ± $s_{\bar{x}}$ (SEM) (95% confidence interval; number of observations). Statistical significance is calculated using Student's t test. N.S.: not significant ($P > 0.05$).

1.0 mm wide microscope fields with the complete thickness of mucosa at 200× magnification. Only immunolabelled cells with visible nuclei (counter-stained with DAPI) were included in quantification.

Serum and tissue gastrin measurements

Serum and tissue samples were collected for measurements of gastrin concentrations from untreated, not fasted animals. Serum samples were taken from the retro-bulbar plexus with capillary pipets.

Antral tissues (0.04–0.08 g wet weight) were collected under a 4× magnifier lens and stored at −70°C until protein preparation. Proteins were extracted and measured for protein concentrations as described earlier (19). Briefly, frozen tissues were homogenized in 5 volumes of lysis buffer (PBS containing 0.2% Triton X-100, 5 mM EDTA, 5 mM EGTA, 100 µm AEBSF, 10 µg/ml leupeptin, 10 µg/ml pepstatin and 10 µg/ml aprotinin) using a Tissumizer homogenizer (Tekmar, Cincinnati, O., USA). The homogenates were centrifuged and supernatants were collected. The protein concentrations were determined by the BCA method (Pierce, Rockford, Il., USA). Sera and tissue protein extracts were stored at −20°C until assayed.

Gastrin concentrations were analysed in duplicates by radioimmunoassay, according to the manufacturer's instructions. The polyclonal antibody, generated against human gastrin, recognizes gastrin-17 I-II forms and partially gastrin-33 forms. It does not react with cholecystokinin. Since there is a 100% homology between the carboxy-terminal 12 amino acids of human and murine gastrin-17 forms (Swiss Prot Database P01350 and P48757, respectively), this antibody reacts with both human and murine gastrins (and potentially precursors). The specificity of the antibody was also confirmed in our hands by immunohistochemistry in mice stomach tissues. Serum gastrin concentration was expressed as pg/ml, tissue gastrin was adjusted to protein content as ng/mg protein.

Statistical methods

Mean ± standard error of mean ($s_{\bar{x}}$) data are presented throughout the results section. Two-tailed two-sample Student's t tests were used for statistical hypothesis testing.

Chemicals

All chemicals, except where otherwise indicated, were purchased from Sigma-Aldrich (Germany): pentobarbital sodium (Nembutal, Phylaxia-Sanofi, Hungary); 4',6-diamidino-2-phenylindole (DAPI); histamine dihydrochloride; pentagastrin (Pentagastrin Injection BP, Cambridge Laboratories, UK); bethanechol (carbonyl-γ-methylcholine Cl); Triton X-100; EDTA; EGTA; AEBSF; leupeptin; pepstatin; aprotinin; BCA protein assay kit (Pierce, Rockford, Il., USA); gastrin radioimmunoassay kit (Gastrin ^{125}I RIA Kit, DiaSorin, Stillwater, Mich., USA); paraformaldehyde (Polysciences, Warrington, Pa., USA); phosphate-buffered saline (PBS); sucrose (ICN Biomedicals, Aurora, O., USA); rat gastrin peptide; rat HDC protein (kind donation of Dr. Lo Persson, Dept. of Physiology, University of Lund, Sweden). Immunohistochemicals are listed in Table I.

Results

Gastric acid secretion

A reduced basal gastric acid output was found in the $HDC^{-/-}$ mice compared with the wild types (Fig. 1A). As a response to exogenous histamine stimulation, the maximal gastric acid output was 2-fold higher in $HDC^{-/-}$ mice than that in $HDC^{+/+}$ (Fig. 1B).

Pentagastrin and bethanechol failed to evoke acid secretion in $HDC^{-/-}$ mice comparable to the wild types (Fig. 1C and 1D). A higher gastric acid output was found after cholinergic stimulus than after pentagastrin stimulation ($P < 0.05$).

Histochemical and morphometric data

The histochemical structure of the stomachs of $HDC^{-/-}$ mice was maintained, although the fundic mucosa of knockouts appeared to be thicker than that of wild types with comparable body weight, giving the impression of being occupied by more parietal cells (Fig. 2).

In knockouts kept on a low-histamine diet morphometric data showed an increased wet whole stomach weight, a

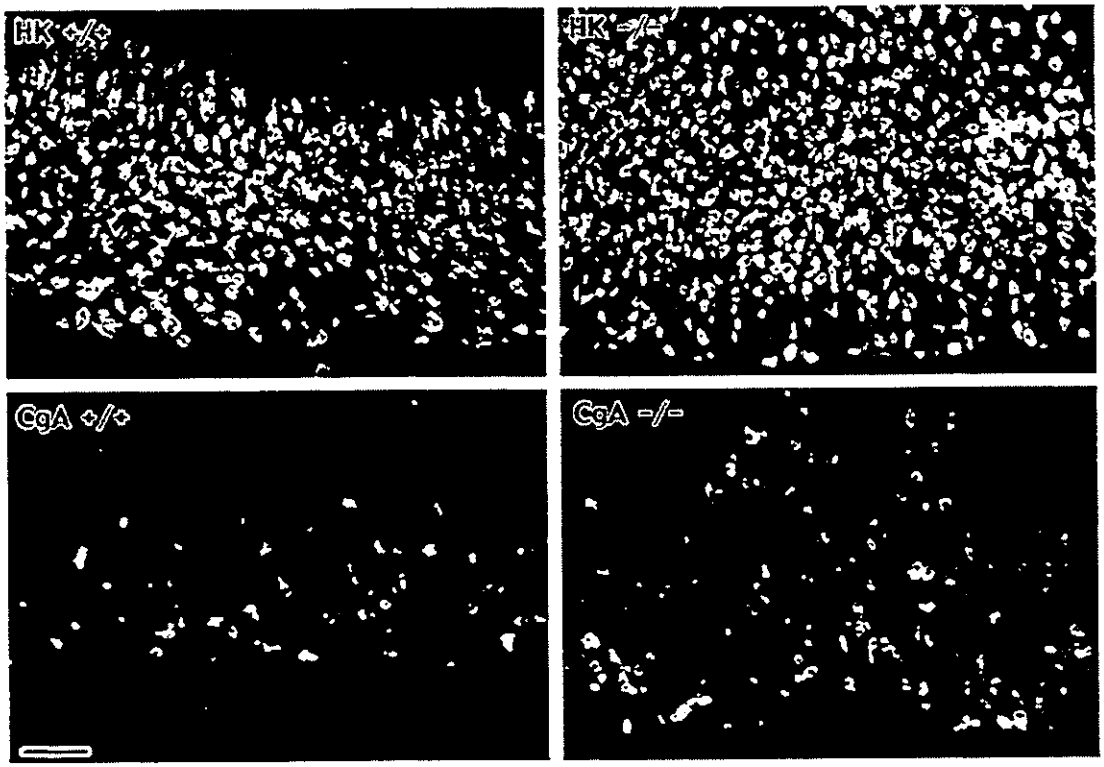

Fig. 2. Histochemical structure of the fundic stomachs of wild-type (+/+) and histidine decarboxylase deficient (−/−) mice. Organization of proton pump (HK) positive parietal and chromagranin A (CgA) positive enterochromaffin-like cells looks similar in wild types and knockouts, although the fundic mucosa of $HDC^{-/-}$ mice appears to be thicker than that of littermate wild types with comparable body weight. Scale bar: 150 μm.

thickened mucosa of fundic stomach and an increased number of parietal cells per field compared to wild types with comparable body weight (Table II).

Unfortunately, quantification of ECL cells failed because our antibody to CgA did not react in paraffin-embedded tissues prepared specifically for cell quantification, not even in wild-type animals. This antibody, however, clearly labelled endocrine cells in our cryostat sections (Fig. 2). Unfortunately, no matching cryostat sections of wild-type and knockout animals were available at this point.

Consistent with observed lack of HDC enzyme activity (7), there was no HDC immunoreactive protein in epithelial cells of the fundic mucosa (even though there were CgA positive ECL cells present) (Fig. 3).

Serum and tissue gastrin measurements

As a potential clue to the increased histamine-induced maximal gastric acid output, and as a possible background to the expanded parietal cell pool, we found an elevated serum gastrin level in $HDC^{-/-}$ mice compared to the wild types (Fig. 4A). The serum gastrin level of $HDC^{-/-}$ mice increased even further after being kept on a low-histamine diet compared to knockouts not deprived of histamine (Fig. 4A). Antral tissues of knockouts contained higher amounts of immunoreactive gastrin than those of wild types (Fig. 4B).

Discussion

The contribution of different regulatory components to gastric acid secretion is still not completely understood. The final in vivo outcome is influenced by multiple interactions and modulators. As reported here, the HDC-deficient mice provide an excellent model for studying the impact of histamine on gastric physiology.

After our previous results in mice kept on a histamine-containing diet (9), we report here secretory and morphometric data of animals maintained on a low-histamine diet. Instead of facing fertility, pregnancy and lactation disturbances and a complexity of developmental consequences in animals kept on a low-histamine diet from birth, we decided to withdraw histamine from the animals after they reached adult age. In our opinion, this model most resembles the human conditions where a normally developed stomach turns achlorhydric in adulthood as a consequence of chronic inflammation or long-term antisecretory treatment.

Histamine content of the stomach is practically zero in the

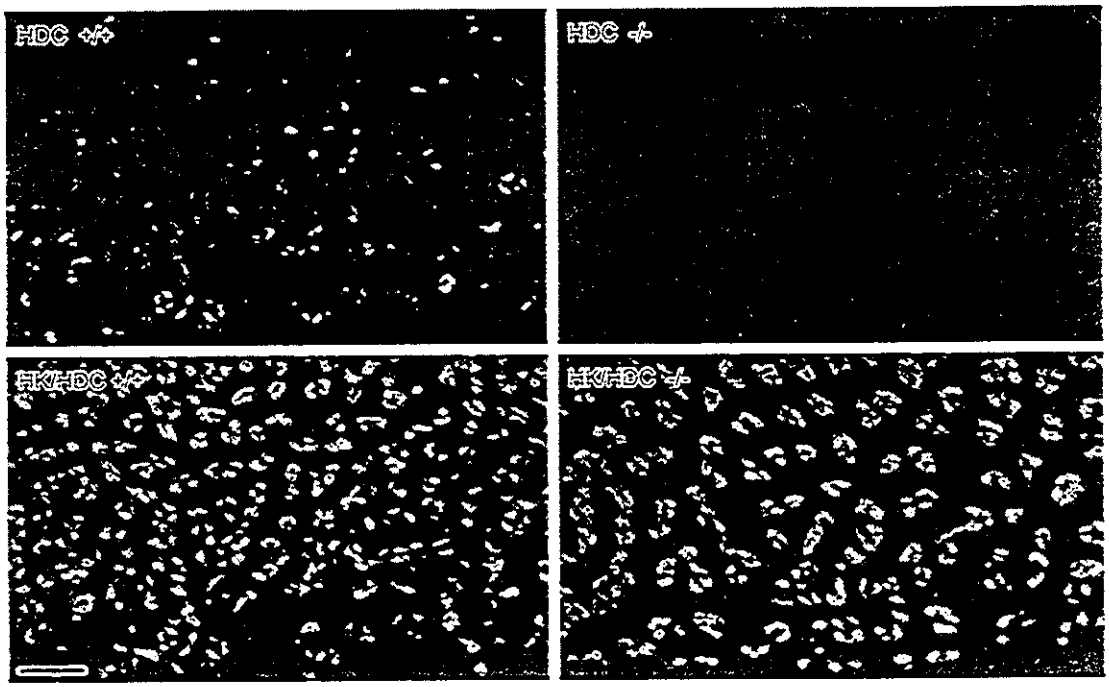

Fig. 3. Histidine decarboxylase (HDC) immunoreactive enterochromaffin-like cells (red labelling) and proton-pump positive parietal cells (HK, green labelling) in the fundic mucosa of wild-type (+/+) and histidine decarboxylase-deficient (−/−) mice. Both signals appear in the double exposure of the *bottom panels*. Consistent with the absence of immunoreactive HDC enzyme, no red colour labelling in the stomach of $HDC^{-/-}$ mice. As demonstrated in Fig. 2, ECL cells are still present in the fundic mucosa of $HDC^{-/-}$ mice. Scale bar: 150 μm.

knockouts after 1 week on a low-histamine diet, while histamine levels remain in the normal range in wild types on such a diet and in knockouts supplemented nutritionally with histamine (7).

We found substantially reduced basal and stimulated gastric acid outputs in HDC-deficient mice maintained on a low-histamine diet (9). The secretory response was superior after administration of high-dose bethanechol than the response after gastrinergic stimulus in HDC-deficient mice, suggesting the existence of a histamine-independent cholinergic secretory pathway (9, 25–27).

Our previous observations on attenuated basal-, gastrin- and cholinergic-stimulated gastric acid secretion, found in young adult animals fed on a histamine-containing diet (9), have been extended here to older $HDC^{-/-}$ animals kept on a low-histamine diet for a prolonged period of time. In this regard we hypothesize that no sufficient escape mechanisms may develop in the $HDC^{-/-}$ animals to compensate for histamine deficiency and restore gastric acid secretion during a prolonged period of time. In other words, our results suggest 1) no alternative pathway of histamine synthesis in $HDC^{-/-}$ mice and 2) insufficient compensatory mechanisms (i.e. elevated serum gastrin level and expanded parietal cell pool) to maintain or restore normal gastric acid secretion.

In our previous paper (9) we demonstrated a maintained structure of gastric mucosa in young adult $HDC^{-/-}$ mice kept on a histamine-containing diet. Our current observations on an expanded parietal cell pool in older, histamine-deprived $HDC^{-/-}$ mice suggest a trophic consequence of prolonged histamine deficiency, potentially through prolonged hypergastrinaemia. Nevertheless, other mechanisms cannot be excluded.

Lack of negative feedback from intragastric acid might explain the elevated gastric tissue and serum concentrations of gastrin, which are, in turn, hypothesized to contribute to the expanded parietal cell pool of the stomach. In this way, gastric acid over-production after exogenous histamine administration might reflect both a continuous stimulatory effect from other arm(s) of gastric acid secretion (as demonstrated here by elevated serum and tissue gastrin levels), and an increased number of parietal cells caused by hypergastrinaemia. However, not one of these changes is able to maintain normal gastric acid secretion—either basal or stimulated—without a sufficient exogenous supply of histamine.

Based on our previous data (9), hypergastrinaemia might develop early in $HDC^{-/-}$ mice. The potential rapid rise of serum gastrin levels through emptying G-cell stores of gastrin as a consequence of withdrawal of dietary histamine with an overnight fasting also has to be addressed in further studies. However, a prolonged period of time might be necessary for expansion of the parietal cell pool.

The $HDC^{-/-}$ mice seem to be a suitable model for studying

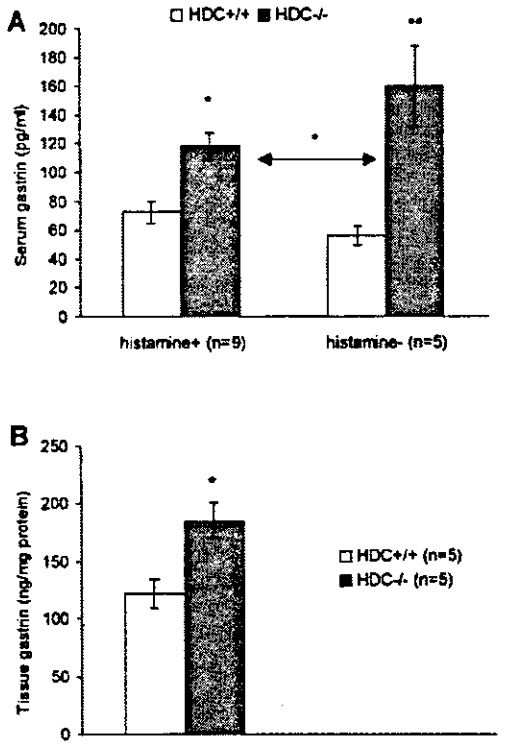

Fig. 4. Elevated serum and tissue gastrin levels in histidine decarboxylase-deficient ($HDC^{-/-}$) mice. Panel A: Elevated serum gastrin level of ($HDC^{-/-}$) mice kept on a histamine-enriched diet (histamine + *left*) increased further after being kept on a low-histamine diet (histamine-*right*). Panel B: Markedly increased antral tissue gastrin levels in $HDC^{-/-}$ mice compared to wild types ($HDC^{+/+}$). $^{*}P < 0.05$; $^{**}P < 0.01$

the effects of long-term achlorhydria in animals as an approach to several human conditions, especially if ECL cell hyperplasia during a prolonged period of a histamine-free diet could be demonstrated in further studies. Anacidity and hypergastrinaemia are shown to increase the risk of gastric malignancies in *men*, and for this reason concerns have been raised regarding long-term antisecretory therapy, particularly with proton-pump inhibitors (28–38). Should gastric tumours develop in achlorhydric ($HDC^{-/-}$) mice because of hypergastrinaemia without any additional genetic/alimentary/infectious factor(s)? Are there other gastrointestinal consequences from the lack of histamine synthesis? These are just a couple of the intriguing issues that will be better understood with the help of the $HDC^{-/-}$ mice.

In summary, we report no restoration of basal, pentagastrin- and bethanechol-stimulated gastric acid secretion in $HDC^{-/-}$ mice kept for a prolonged period of time on a low-histamine diet and with a double histamine-induced maximal gastric acid secretory capacity. Furthermore, our studies also conclude the development of an expanded parietal cell pool in $HDC^{-/-}$ mice when fed on a low-histamine diet. This expansion of the parietal cell pool might be explained by a trophic effect of sustained hypergastrinaemia—although other factors need to be further investigated. The $HDC^{-/-}$ mice seem to be a suitable model for studying the effects of prolonged achlorhydria and consequent hypergastrinaemia as an approach to human conditions such as atrophic gastritis or long-term antisecretory therapies.

Acknowledgements

These studies were partially supported through the Hungarian OTKA (Grant T025847) and ETT (Grant T-01 086/99). Béla Hunyady was funded through a János Bolyai research grant from the Hungarian Academy of Sciences. We thank Dr. Lee E. Eiden (National Institute of Mental Health, Bethesda, Md., USA) for kindly donating the antibody to chromogranin A. Special thanks are extended to Helferik Frigyesné, Vidra Zsuzsanna and Czérna Emke for their assistance.

References

1. Black JW. Neurochemical control of oxyntic cell secretion. Hepato-Gastroenterol 1990;37 Suppl 1:31–5.
2. Daugherty DF, Lucey MR, Yamada T. Gastric secretion. In: Yamada T, editor. Textbook of gastroenterology. Philadelphia: JB Lippincott; 1992:233–64.
3. Rangachari PK. Histamine: mercurial messenger in the gut [editorial]. Am J Physiol 1992;262:G1–13.
4. Kurbel S, Kurbel B. The role of gastric mast cells, enterochromaffin-like cells and parietal cells in the regulation of acid secretion. Med Hypotheses 1995;45:539–42.
5. Hakanson R, Chen D, Andersson K, Monstein HJ, Zhao CM, Ryberg B, et al. The biology and physiology of the ECL cell. Yale J Biol Med 1994;67:123–34.
6. Dockray GJ, Varro A, Dimaline R. Gastric endocrine cells: gene expression, processing, and targeting of active products. Physiol Rev 1996;76:767–98.
7. Ohtsu H, Tanaka S, Terui T, Hori Y, Makabe-Kobayashi Y, Pejler G, et al. Mice lacking histidine decarboxylase exhibit abnormal mast cells. FEBS Lett 2001;502:53–6.
8. Viguera E, Trelles O, Urdiales JL, Mates JM, Sanchez-Jimenez F. Mammalian L-amino acid decarboxylases producing 1,4-diamines: analogies among differences. Trends Biochem Sci 1994;19:318–9.
9. Tanaka S, Hamada K, Yamada N, Sugita Y, Tonai S, Hunyady B, et al. Gastric acid secretion in L-histidine decarboxylase-deficient mice. Gastroenterology 2002;122:145–55.
10. Friis-Hansen L, Sundler F, Li Y, Gillespie PJ, Saunders TL, Greenson JK, et al. Impaired gastric acid secretion in gastrin-deficient mice. Am J Physiol 1998;274(3 Pt 1):G561–8.
11. Bhattacharjee M, Bose AK, Banerjee RK. Histamine H2-receptor mediated stimulation of gastric acid secretion by mercaptomethylimidazole. Biochem Pharmacol 1989;38:907–14.
12. Langhans N, Rindi G, Chiu M, Rehfeld JF, Ardman B, Beinborn M, et al. Abnormal gastric histology and decreased acid production in cholecystokinin-B/gastrin receptor-deficient mice. Gastroenterology 1997;112:280–6.
13. Barocelli E, Chiavarini M, Ballabeni V, Barlocco D, Vianello P, Dal PV, et al. Study of the antisecretory and antiulcer mechanisms of a new indenopirydazinone derivative in rats. Pharmacol Res 1997;35:487–92.
14. Improta G, Broccardo M. Inhibitory role on gastric secretion of a central NK-3 tachykinin receptor agonist, senktide. Peptides 1991;12:1433–4.
15. Facer P, Bishop AE, Lloyd RV, Wilson BS, Hennessy RJ, Polak

JM. Chromogranin: a newly recognized marker for endocrine cells of the human gastrointestinal tract. Gastroenterology 1985; 89:1366–73.
16. Lenz HJ, Mortrud MT, Rivier JE, Brown MR. Calcitonin gene related peptide inhibits basal, pentagastrin, histamine, and bethanecol stimulated gastric acid secretion. Gut 1985;26:550–5.
17. Lloris JM, Bolant B, Gimeno L, Cejalvo D, Gimeno LO, Calvo MA, et al. Gastric juice and analysis of basal and stimulated secretion following treatment with rice-bran oil. Res Commun Chem Pathol Pharmacol 1991;74:245–8.
18. Shoji E, Okumura T, Kohgo Y. Intraduodenal lipid does not inhibit acid secretion in OLETF rats not expressing CCK-A receptor gene. Dig Dis Sci 1996;41:2174–9.
19. Hunyady B, Zólyomi A, Hoffman BJ, Mezey É. Gastrin-producing endocrine cells: a novel source of histamine in the rat stomach. Endocrinology 1998;139:4404–15.
20. Hunyady B, Mezey É, Pacak K, Palkovits M. Identification of endogenous peroxidase-containing cells as eosinophils in the gastrointestinal system. Histochemistry 1996;106:447–56.
21. Hunyady B, Krempels K, Harta G, Mezey É. Immunohistochemical signal amplification by catalyzed reporter deposition and its application in double immunostaining. J Histochem Cytochem 1996;44:1353–62.
22. Smolka A, Swiger KM. Site-directed antibodies as topographical probes of the gastric H,K-ATPase alpha-subunit. Biochim Biophys Acta 1992;1108:75–85.
23. Coruzzi G, Adami M, Bertaccini G. Gastric antisecretory activity of lansoprazole in different experimental models: comparison with omeprazole. Gen Pharmacol 1995;26:1027–32.
24. Erickson JD, Schafer MK, Bonner TI, Eiden LE, Weihe E. Distinct pharmacological properties and distribution in neurons and endocrine cells of two isoforms of the human vesicular monoamine transporter. Proc Natl Acad Sci USA 1996;93:5166–71.
25. Sandvik AK, Marvik R, Dimaline R, Waldum HL. Carbachol stimulation of gastric acid secretion and its effects on the parietal cell. Br J Pharmacol 1998;124:69–74.
26. Sandor A, Kidd M, Lawton GP, Miu K, Tang LH, Modlin IM. Neurohormonal modulation of rat enterochromaffin-like cell histamine secretion. Gastroenterology 1996;110:1084–92.
27. Soll AH. Secretagogue stimulation of [14C]aminopyrine accumulation by isolated canine parietal cells. Am J Physiol 1980;238:G366–75.
28. Sculco D, Bilgrami S. Pernicious anemia and gastric carcinoid tumor: case report and review. Am J Gastroenterol 1997;92: 1378–80.
29. Soybel DI, Modlin IM. Sustained suppression of gastric secretion and the risk of neoplasia in the gastric mucosa. Am J Gastroenterol 1991;86:1713–9.
30. Wormsley KG. Therapeutic achlorhydria and risk of gastric cancer. Gastroenterol Jpn 1989;24:585–96.
31. Creutzfeldt W. The achlorhydria-carcinoid sequence: role of gastrin. Digestion 1988;39:61–79.
32. Penston J, Wormsley KG. Achlorhydria: hypergastrinaemia: carcinoids—a flawed hypothesis? Gut 1987;28:488–505.
33. Solcia E, Capella C, Sessa F, Rindi G, Cornaggia M, Riva C, et al. Gastric carcinoids and related endocrine growths. Digestion 1986;35 Suppl 1:3–22:3–22.
34. Szabo I, Rumi G, Bodis B, Nemeth P, Mozsik G. Gastrin and pentagastrin enhance the tumour proliferation of human stable cultured gastric adenocarcinoma cells. J Physiol Paris 2000;94: 71–4.
35. Bordi C, D'Adda T, Azzoni C, Pilato FP, Caruana P. Hypergastrinemia and gastric enterochromaffin-like cells. Am J Surg Pathol 1995;19 Suppl 1:S8–19.
36. Larsson H, Hakanson R, Mattsson H, Ryberg B, Sundler F, Carlsson E. Omeprazole: its influence on gastric acid secretion, gastrin and ECL cells. Toxicol Pathol 1988;16:267–72.
37. Solcia E, Rindi G, Havu N, Elm G. Qualitative studies of gastric endocrine cells in patients treated long-term with omeprazole. Scand J Gastroenterol 1989;166 Suppl:129–39.
38. Hunt RH. The protective role of gastric acid. Scand J Gastroenterol 1988;146 Suppl:34–9.

Received 11 April 2002
Accepted 21 October 2002

Am J Physiol Renal Physiol 284: F1164–F1170, 2003.
First published March 11, 2003; 10.1152/ajprenal.00441.2002.

Expression of the prostaglandin F receptor (FP) gene along the mouse genitourinary tract

Osamu Saito,[1] Youfei Guan,[1] Zhonghua Qi,[1] Linda S. Davis,[1] Martin Kömhoff,[2] Yukihiko Sugimoto,[3] Shuh Narumiya,[3] Richard M. Breyer,[1] AND Matthew D. Breyer[1]

[1]Division of Nephrology, Department of Medicine, Vanderbilt University Veterans Affairs Medical Center, Nashville, Tennessee 37212; and Departments of [3]Pharmacology, Faculty of Medicine, and [2]Physiological Chemistry and Faculty of Pharmaceutical Sciences, Kyoto University, Kyoto, Japan 606

Submitted 30 December 2002; accepted in final form 9 February 2003

Saito, Osamu, Youfei Guan, Zhonghua Qi, Linda S. Davis, Martin Kömhoff, Yukihiko Sugimoto, Shuh Narumiya, Richard M. Breyer, and Matthew D. Breyer. Expression of the prostaglandin F receptor (FP) gene along the mouse genitourinary tract. *Am J Physiol Renal Physiol* 284: F1164–F1170, 2003. First published March 11, 2003; 10.1152/ajprenal.00441.2002.—$PGF_{2\alpha}$ is one of the major prostanoids produced by the kidney. The cellular effects of $PGF_{2\alpha}$ are mediated by a G protein-coupled transmembrane receptor designated the FP receptor. Both in situ hybridization and β-galactosidase knocked into the endogenous FP locus were used to determine the cellular distribution of the mouse FP receptor. Specific labeling was detected in the kidney, ovary, and uterus. Abundant FP expression in ovarian follicles and uterus is consistent with previous reports of failed parturition in FP−/− mice. In the kidney, coexpression of the mFP mRNA with the thiazide-sensitive cotransporter defined its expression in the distal convoluted tubule (DCT). FP receptor was also present in aquaporin-2-positive cortical collecting ducts (CCD). No FP mRNA was detected in glomeruli, proximal tubules, or thick ascending limbs. Intrarenal expression of the FP receptor in the DCT and CCD suggests an important role for the FP receptor regulating water and solute transport in these segments of the nephron.

dinoprost; nephron; natriuresis; water

PROSTANOIDS, including PGE_2, PGD_2, prostacyclin (PGI_2), TxA_2, and $PGF_{2\alpha}$, modulate a diverse spectrum of physiological processes, including reproduction, inflammation, microvascular resistance, and epithelial ion transport rates (7, 33). Despite originating from a common precursor, PGH_2, the effects of these derivative prostanoids may either oppose each other, as in the case of the prothrombotic action of TxA_2 vs. the antithrombotic effects of PGI_2 (16), or exert functionally complementary effects such as the smooth muscle constrictor effects of TxA_2 and $PGF_{2\alpha}$ (48). These cellular and physiological effects are mediated by the selective interaction of each prostanoid with unique G protein-coupled receptors (GPCRs) (8, 33, 46). Genetic disruption of GPCR prostanoid receptors has not only firmly established roles for these receptors as critical mediators of prostanoid action, but it also revealed significant new biology related to the roles of prostaglandins (33, 46). In the case of the FP receptor for $PGF_{2\alpha}$, these studies revealed that the FP receptor is highly expressed in the ovary and its function is essential for normal parturition (47).

The FP receptor is also highly expressed in the kidney (2, 44). Furthermore, $PGF_{2\alpha}$ is a major product of cyclooxygenase-mediated arachidonate metabolism in the kidney (14), and renal synthesis of $PGF_{2\alpha}$ is regulated by sodium depletion, potassium depletion, and adrenal steroids (35, 40). Infusion of exogenous $PGF_{2\alpha}$ modulates renal salt excretion and urine flow (42). Despite this evidence supporting a role for the FP receptor in the kidney, the intrarenal sites of expression or mechanism of these $PGF_{2\alpha}$-activated GPCRs in the kidney remain poorly characterized. The purpose of the present studies was to map the intrarenal distribution of the FP receptor in the kidney.

METHODS

Generation of RNA fragments. RNA probes were generated by RT-PCR to amplify a 399-bp fragment spanning the 5′-UTR to Arg^{100} in the coding region of the mouse FP receptor cDNA from kidney RNA. The sense primer was 5′-AACCACTCAGTGGCTCAGGA-3′, and the antisense primer was 5′-GCGGATCCAGTCTTTATC3′. The identity of the amplified product was directly confirmed by sequencing and alignment with the mouse FP receptor (BLAST, NCBI) and ligated into the transcription vector pCR2.1 (Invitrogen). The two distinct clones were isolated, which allowed transcription of either the sense or antisense cDNAs using the T7 promoter. The plasmids were linearized and RNAs transcribed from the flanking T7 promoter in the presence of [α-^{35}S]UTP. RNA (5×10^5 cpm/μl) was used for in situ hybridization.

Tissue preparation. C57BL/6J mice weighing between 20 and 30 g were anesthetized using intraperitoneal ketamine and xylazine (200 mg and 15 mg/kg, respectively). After surgical anesthesia was achieved, mice were killed by cervical dislocation and kidney, stomach, liver, ovary, and uterus were harvested.

For in situ hybridization studies, tissues were fixed in 4% paraformaldehyde. Tissues were imbedded in paraffin and

Address for reprint requests and other correspondence: M. D. Breyer, Division of Nephrology and Dept. of Medicine, Vanderbilt Univ., F427-ACRE Bldg., Dept. of Veterans Affairs Medical Center, Nashville, TN 37212 (E-mail: Matthew.Breyer@vanderbilt.edu).

The costs of publication of this article were defrayed in part by the payment of page charges. The article must therefore be hereby marked "*advertisement*" in accordance with 18 U.S.C. Section 1734 solely to indicate this fact.

7-μm sections were cut. Before hybridization, sections were deparaffinized, refixed in paraformaldehyde, treated with proteinase K (20 μg/ml), washed with PBS, refixed in 4% paraformaldehyde, and treated with triethanolamine plus acetic anhydride (0.25% vol/vol). Finally, sections were dehydrated in 100% ethanol.

Anti-sense RNA was hybridized to the sections at 50–55°C for ~18 h as described previously (11). After hybridization, sections were washed at 50°C in 5× SSC + 10 mM β-mercaptoethanol for 30 min. This was followed by a wash in 50% formamide, 2× SSC, and 100 mM β-mercaptoethanol for 60 min. After additional washes in 10 mM TRIS, 5 mM EDTA, 500 mM NaCl (TEN), sections were treated with RNase (10 μg/ml), at 37°C for 30 min, followed by another wash in TEN (37°C). Sections were then washed twice in 2× SSC and then twice in 0.1× SSC (50°C). Slides were dehydrated with graded ethanols containing 300 mM ammonium acetate.

For detection of the hybridized probe, slides were dipped in photo emulsion (Ilford K5, Knutsford, UK) diluted 1:1 with 2% glycerol/water and exposed for 7 days at 4°C. After development in Kodak D19, slides were counterstained with hematoxylin and eosin. Photomicrographs were taken using a Zeiss Axioskop using both bright- and darkfield optics.

Preparation of tissue for β-galactosidase staining and immunohistochemistry. Multiple organs including liver, spleen, stomach, duodenum, lung, and kidneys of the double transgenic mice were harvested at death. After fixation with 4% paraformaldehyde plus 0.25% glutaraldehyde in PBS for 2 h at 4°C, tissue sections were cut with a vibratome into 200-μm slices. To detect β-galactosidase (β-gal) activity, these slices were bathed in permeabilization solution (2 mM $MgCl_2$, 0.01% sodium deoxycholate, 0.02% NP-40 in PBS) for 30 min × 2 and then stained with 1 mg/ml 5-bromo-4-chloro-3-indolyl-D-galactopyranoside (X-gal; Sigma, St. Louis, MO) in staining solution (2 mM $MgCl_2$, 5 mM potassium ferricyanide, potassium ferrocyanide, 20 mM Tris, pH 7.4 in PBS) at room temperature in the dark for 48 h (5, 36). Tissues were washed, dehydrated through graded ethanol series, and embedded in paraffin, using standard procedures. Serial 5-μm sections were cut and examined by light microscopy.

Immunostaining. To define the nephron segments that expressed FP receptor mRNA, in situ hybridization was followed by immunostaining of the tissue sections with a rabbit anti-collecting duct antibody or a goat anti-human Tamm-Horsfall antibody, which specifically recognizes medullary and cortical thick ascending limb (mTAL and cTAL) as well as the early portion of the distal tubule. To define the β-gal-positive nephron segments, sections were co-stained using a goat anti-human Tamm-Horsfall antibody (1:2,500, Organon-Technika) that specifically recognizes mTAL and cTAL as well as the early portion of the distal tubule (28, 49). A commercially available anti-aquaproin-2 (AQP2) antibody was used to specifically identify collecting duct principal cells (AQP21-A, Anti-Rat AQP2 IgG no. 2, Alpha Diagnostic International, San Antonio, TX) (26). To define distal convoluted tubule segments (DCT), an anti-thiazide-sensitive NaCl cotransporter (TSC) antibody was used [generously provided by Dr. M. Knepper (30)]. Staining was localized using a biotinylated anti-IgG secondary antibody applied to β-gal-stained sections. Biotin was identified using streptavidin coupled to horseradish peroxidase and was visualized with diaminiobenzidine (Vector Vectastain ABC kit). Sections were viewed and imaged with a Zeiss Axioskop and Spot-Cam digital camera (diagnostic instruments).

RESULTS

Intrarenal distribution of the FP receptor. Autoradiograms of the kidney, with an anti-sense FP receptor riboprobe (Fig. 1), showed intense labeling of subpopulations of epithelial tubules in the renal cortex. No specific labeling was obtained with a sense mRNA probe (data not shown). There was light and diffuse labeling of the outer medulla. There was no detectable labeling of the papilla. A similar pattern of FP mRNA

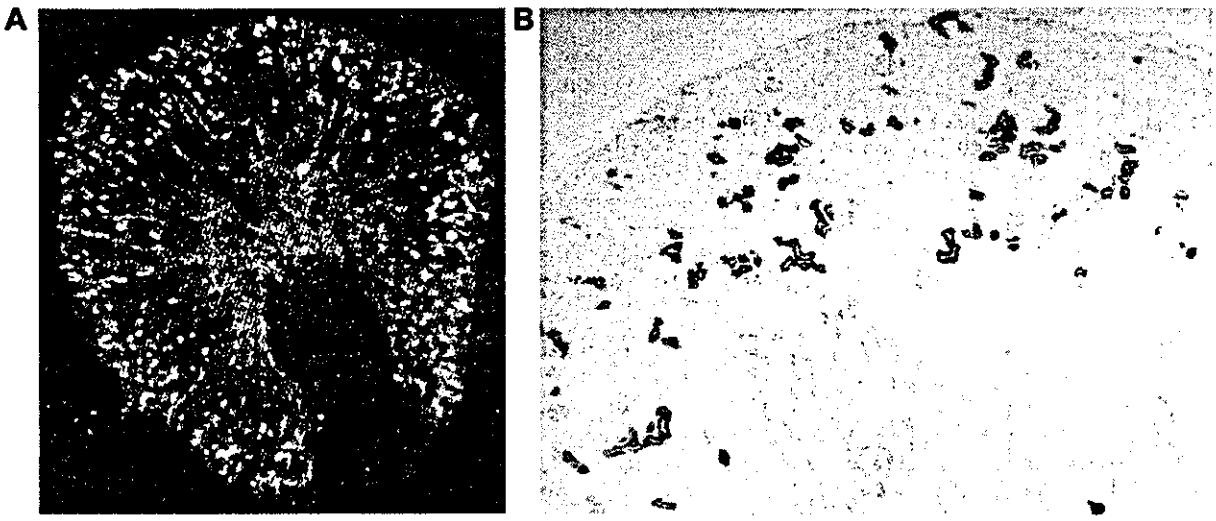

Fig. 1. Expression of FP receptor mRNA in kidney. *A*: ×10 darkfield photomicrograph of an in situ hybridization using the mouse FP receptor mRNA as a riboprobe. The white grains indicate areas of message expression that predominate in the cortex. *B*: ×50 photomicrograph of a kidney from an FP +/− mouse. The blue reaction product identifies structures in which β-galactosidase activity is present in cells, marking active transcription of the lacZ gene knocked into the endogenous FP receptor locus in mice.